Carderock Division
Naval Surface Warfare Center
9500 MacArthur Blvd.
West Bethesda, MD 20817-5700

NSWCCD-SIG-97/256-7030 September 1997

Signatures Directorate
Research and Development Report

PRIMITIVE COMPARISON OF THE SIGNAL-TO-NOISE RATIOS OF PRESSURE AND VELOCITY PLANAR ARRAYS

by

G. Maidanik
K. Becker

NSWCCD-SIG-97/256-7030 September 1997 Primitive Comparison of the Signal-to-Noise Ratios of Pressure and Velocity Planar Arrays

SECURITY CLASSIFICATION OF THIS PAGE

REPORT DOCUMENTATION PAGE

Form Approved OMB No. 0704-0188

1a. REPORT SECURITY CLASSIFICATION Unclassified	1b. RESTRICTIVE MARKINGS None
2a. SECURITY CLASSIFICATION AUTHORITY	3. DISTRIBUTION / AVAILABILITY OF REPORT Approved for public release. Distribution is unlimited.
2b. DECLASSIFICATION/DOWNGRADING SCHEDULE	
4. PERFORMING ORGANIZATION REPORT NUMBER(S) NSWCCD-SIG-97/256-7030	5. MONITORING ORGANIZATION REPORT NUMBER(S)
6a. NAME OF PERFORMING ORGANIZATION NSWC, Carderock Division 6b. OFFICE SYMBOL (*If applicable*) Code 7030	7a. NAME OF MONITORING ORGANIZATION
6c. ADDRESS (*City, State, and ZIP Code*) 9500 MacArthur Blvd. West Bethesda, MD 20817-5700	7b. ADDRESS (*City, State, and ZIP Code*)
8a. NAME OF FUNDING/SPONSORING ORGANIZATION 8b. OFFICE SYMBOL (*If applicable*)	9. PROCUREMENT INSTRUMENT IDENTIFICATION NUMBER
8c. ADDRESS (*City, State, and ZIP Code*)	10. SOURCE OF FUNDING NUMBERS PROGRAM ELEMENT NO. / PROJECT NO. / TASK NO. / WORK UNIT ACCESSION NO.

11. TITLE (*Include Security Classification*)
Primitive Comparison of the Signal-to-Noise Ratios of Pressure and Velocity Planar Arrays

12. PERSONAL AUTHOR(S)
G. Maidanik and K.J. Becker

13a. TYPE OF REPORT	13b. TIME COVERED	14. DATE OF REPORT (*Year, Month, Day*)	15. PAGE COUNT
Research and Development	FROM 970701 TO 970930	1997 September 30	80

16. SUPPLEMENTARY NOTATION

17. COSATI CODES			18. SUBJECT TERMS (*Continue on reverse if necessary and identify by block number*)
FIELD	GROUP	SUB-GROUP	Filtering Efficiency; Pressure Array; Velocity Array; Active and Passive Filtering; Turbulent Boundary Layer

19. ABSTRACT (*Continue on reverse if necessary and identify by block number*)

The combined filtering efficiency of a pressure array and a velocity array, both flush mounted in a plane boundary, are derived and stated. The combined filtering efficiency is factorized into active and passive filtering efficiencies. The active filtering efficiency for the pressure array and for the velocity array are assumed to be identical except for a factor of the square of the characteristic impedance of the fluid that occupies the semi-infinite space above the boundary. This active filtering efficiency is related to the sensitivity of the transducers in the array and to the wave vector on the boundary to which the array is steered. The difference between the filtering efficiency in the pressure array and that in the velocity array lies in the respective passive filtering efficiencies. This difference is used to assess the signal-to-noise ratio pertaining to these two arrays; the pressure array and the velocity array. Then an estimate is performed as to the advantage or the disadvantage that the pressure array may have compared with the velocity array. This estimate is made more explicit by considering the spectral density of the noise to be closely related to that of a turbulent boundary layer (TBL).

20. DISTRIBUTION / AVAILABILITY OF ABSTRACT	21. ABSTRACT SECURITY CLASSIFICATION
☒ UNCLASSIFIED/UNLIMITED ☐ SAME AS RPT. ☐ DTIC USERS	Unclassified
22a. NAME OF RESPONSIBLE INDIVIDUAL Maidanik, G.	22b. TELEPHONE (*Include Area Code*) (301)227-1292 22c. OFFICE SYMBOL NSWCCD 7030

DD Form 1473, JUN 86 *Previous editions are obsolete.*

SECURITY CLASSIFICATION OF THIS PAGE

CONTENTS

ABSTRACT

The combined filtering efficiency of a pressure array and a velocity array, both flush mounted in a plane boundary, are derived and stated. The combined filtering efficiency is factorized into active and passive filtering efficiencies. The active filtering efficiency for the pressure array and for the velocity array are assumed to be identical except for a factor of the square of the characteristic impedance of the fluid that occupies the semi-infinite space above the boundary. This active filtering efficiency is related to the sensitivity of the transducers in the array and to the wave vector on the boundary to which the array is steered. The difference between the filtering efficiency in the pressure array and that in the velocity array lies in the respective passive filtering efficiencies. This difference is used to assess the signal-to-noise ratio pertaining to these two arrays; the pressure array and the velocity array. Then an estimate is performed as to the advantage or the disadvantage that the pressure array may have compared with the velocity array. This estimate is made more explicit by considering the spectral density of the noise to be closely related to that of a turbulent boundary layer (TBL).

INTRODUCTION

It is assumed that the incident pressure on a boundary is spatially and temporally stationary so that the pressure can be defined in terms of its spectral density $\Phi(\underset{\sim}{k},\omega)$, where $(\underset{\sim}{k})$ is the wave vector variable in the plane of the boundary and (ω) is the frequency variable. It is also assumed that the spectral components in the signal are uncorrelated with the spectral components of the (unwanted) noise so that

$$\Phi(\underset{\sim}{k},\omega) = \Phi_S(\underset{\sim}{k},\omega) + \Phi_N(\underset{\sim}{k},\omega) ; \qquad \underset{\sim}{k} = \{k_x, k_y\} , \tag{1}$$

where $\Phi_S(\underset{\sim}{k},\omega)$ and $\Phi_N(\underset{\sim}{k},\omega)$ are the spectral densities of the signal and noise, respectively. The output $O(\underset{\sim}{k}_s,\omega)$ of the boundary array to the incident spectral density $\Phi(\underset{\sim}{k},\omega)$ may be formally expressed in the form

$$O(\underset{\sim}{k}_S,\omega) \;=\; \int d\underset{\sim}{k}\;\; J(\underset{\sim}{k}_S \mid \underset{\sim}{k},\omega)\;\; \Phi(\underset{\sim}{k},\omega)\;; \qquad d\underset{\sim}{k} \;=\; dk_x\;\; dk_y\;;$$

$$J(\underset{\sim}{k}_S \mid \underset{\sim}{k},\omega) \;=\; A(\underset{\sim}{k}_S \mid \underset{\sim}{k},\omega)\;\; D(\underset{\sim}{k},\omega)\;; \qquad \underset{\sim}{k}_S \;=\; \{k_{sx},k_{sy}\}\;, \tag{2}$$

where $D(\underset{\sim}{k},\omega)$ is the filtering efficiency of the boundary -- the passive filtering efficiency-- and $A(\underset{\sim}{k}_S \mid \underset{\sim}{k},\omega)$, is the filtering efficiency of the array -- the active filtering efficiency -- steered to the specific wave vector $(\underset{\sim}{k}_S)$. The quantity $J(\underset{\sim}{k}_S \mid \underset{\sim}{k},\omega)$ is the combined filtering efficiency of the flush mounted array. Both the passive and the active filtering efficiencies are designed into the array in order to maximize the signal-to-noise ratio R_N^S, which is given by

$$R_N^S(\underset{\sim}{k}_S,\omega) \;=\; [O_S(\underset{\sim}{k}_S,\omega) \;/\; O_N(\underset{\sim}{k}_S,\omega)]\;, \tag{3}$$

where, from Eqs. (1) and (2), one finds that

$$O_S(\underset{\sim}{k}_S,\omega) \;=\; \int d\underset{\sim}{k}\;\; A(\underset{\sim}{k}_S \mid \underset{\sim}{k},\omega)\;\; D(\underset{\sim}{k},\omega)\;\; \Phi_S(\underset{\sim}{k},\omega)\;, \tag{4a}$$

$$O_N(\underset{\sim}{k}_S,\omega) \;=\; \int d\underset{\sim}{k}\;\; A(\underset{\sim}{k}_S \mid \underset{\sim}{k},\omega)\;\; D\mid(\underset{\sim}{k},\omega)\;\; \Phi_N(\underset{\sim}{k},\omega)\;. \tag{4b}$$

Thus, the maximization of R_N^S requires the combined filtering efficiency $J(\underset{\sim}{k}_S \mid \underset{\sim}{k},\omega)$ $\{=[A(\underset{\sim}{k}_S \mid \underset{\sim}{k},\omega)\;\; D\mid(\underset{\sim}{k},\omega)]\}$ to favorably accept the signal compon ents $\Phi_S(\underset{\sim}{k},\omega)$ and to simultaneously reject the noise components $\Phi_N(\underset{\sim}{k},\omega)$. For example, it is a fact that the signal $\Phi_S(\underset{\sim}{k},\omega)$ is supersonic; i.e.,

$$\Phi_S(\underset{\sim}{k},\omega) \;=\; \Phi_{0S}(\underset{\sim}{k},\omega)\;\; U\;\; [1-(kc/\omega)]\;, \tag{5}$$

where U is the unit step function and $k = |\underset{\sim}{k}|$. It becomes necessary, therefore, to ensure that the combined filtering efficiency $J(\underset{\sim}{k}_S \mid \underset{\sim}{k}, \omega)$ is supersonically viable. On the other hand, the noise $\Phi_N(\underset{\sim}{k}, \omega)$ possesses, by definition, the entire complement of the subsonic components in the incident spectral density on the boundary. Thus, although there may be noise components that reside in the supersonic range; i.e.,

$$\Phi_N(\underset{\sim}{k}, \omega) = \Phi_{0N}(\underset{\sim}{k}, \omega)\ U[1-(kc/\omega)]$$

$$+\ \Phi_{1N}(\underset{\sim}{k}, \omega)\ U[(kc/\omega)-1]\ , \qquad (6)$$

the combined filtering efficiency $J(\underset{\sim}{k}_S \mid \underset{\sim}{k}, \omega)$ is the better the more it rejects subsonic components. That betterment, however, should not be derived at the expense of the acceptance in the supersonic range. The supersonic components in the noise; namely, $\Phi_{0N}(\underset{\sim}{k}, \omega)\ U[1-(kc/\omega)]$ are not readily distinguishable from those of the signal. To selectively make this distinction between these two types of supersonic components; the supersonic signal components and the supersonic noise components, the active filtering efficiency $A(\underset{\sim}{k}_S \mid \underset{\sim}{k}, \omega)$ must attain a degree of sophistication, notwithstanding that this filtering efficiency may be called upon to further enhance the rejection of the subsonic components above and beyond that provided by the passive filtering efficiency $D(\underset{\sim}{k}\,\omega)$. Hypothetical but instructive illustrations of the filtering efficiencies $A(\underset{\sim}{k}_S \mid \underset{\sim}{k}, \omega)$ and $D(\underset{\sim}{k}, \omega)$ and their utility are sketched in Fig. 1. The statements just presented are reflected in these illustrations. The incident spectral density is illustrated in Fig. 1a. The signal is confined to a narrow spectral region in the supersonic range. That narrow spectral region is centered about $\{\underset{\sim}{k}_S, \omega\}$. The noise, on the other hand, possesses supersonic and subsonic components. However, the larger portion of the components of the noise reside in the subsonic range. A typical passive filtering efficiency $D(\underset{\sim}{k}, \omega)$ is depicted in Fig. 1b. This filtering efficiency accepts well in the supersonic range and rejects particularly well at the

higher-subsonic range. The rejection at the higher-subsonic range is usually achieved by an introduction of a blanket on the boundary. A blanket is a device that hardly changes the passive filtering efficiency of the unblanketed array in the supersonic range but exponentially reduces this passive filtering efficiency in the high-subsonic range. The exponential reduction is proportional to the thickness of the blanket. A typical active filtering efficiency $A(\underset{\sim}{k}_S \mid \underset{\sim}{k}, \omega)$ is depicted in Fig. 1c. The selected acceptance at $\{\underset{\sim}{k}_S, \omega\}$ and the suppression outside this spectral region are clearly illustrated in Fig 1c; the suppression outside the spectral region $\{\underset{\sim}{k}_S, \omega\}$ is enhanced, in the active filtering efficiency, largely by an array shading. The combined filtering efficiency is illustrated in Fig 1d. The combined filtering efficiency is particularly effective in rejecting the detrimental noise component that reside in the wave vector range depicted in Fig. 1a at the wave vector $\{k_x, k_y\} = \{(\omega / U_c),\ 0\}$, so that in this region $k = (\omega / U_c)$, where $M_c = (U_c / c)$ is a Mach number with respect to the speed of sound (c). That Mach number is small compared with unity; $M_c << 1$. This character in the noise is reminiscent of the noise generated by a turbulent boundary layer (TBL) in which the convective velocity is $\underset{\sim}{U}_c$. Figure 1 suggests that the combined filtering efficiency $J(\underset{\sim}{k}_S \mid \underset{\sim}{k}, \omega)$, as illustrated, is particularly effective against the convective ridge in the noise of a TBL. On the other hand, the combined filtering efficiency is not correspondingly effective against the noise components that reside in the supersonic region. If these noise components are not too prevalent, the combined filtering efficiency may be adequate for the task. Otherwise, as already mentioned, a more sophisticated active array filtering efficiency may be required to take care of the suppression of supersonic noise components; e.g., and adaptive filtering efficiency.

The foregoing exposition in this report is intended to serve merely as a review of material assumed familiar to the reader. In this way the intended subject matter of this report can be introduced more directly and without overly dwelling on concepts that are covered above and in other publications and reports [1-12]. The present report contrasts

the performance of two arrays types. One is composed of embedded "pressure transducers" that are flush mounted in the boundary and the second of "velocity transducers." Both arrays are assumed to be subjected to the same incident pressure spectral density $\Phi_p(\underset{\sim}{k},\omega)$. However, each array is designed to maximize the signal-to-noise ratio $R_N^S(\omega)$; $R_{pN}^S(\omega)$ for the pressure array and $R_{vN}^S(\omega)$ for the velocity array.

I. THE PASSIVE FILTERING EFFICIENCY FOR A PRESSURE ARRAY

The boundary faced by a semi-infinite spaced filled with a fluid and the coordinate system to be used are sketched in Fig. 2. The pressure p_b and the velocity v_b on the boundary are related, in terms of the conservation of momentum at the fluid-boundary interface, in the form

$$\rho(\partial v_b / \partial t) = -(\partial p_b / \partial z) , \tag{7}$$

where (ρ) is the fluid density, (t) is the temporal variable and (z) is the spatial variable normal to the boundary. [cf. Fig. 2.] In spectral space Eq. (7) assumes the form

$$[P_b(\underset{\sim}{k},\omega) / V_b(\underset{\sim}{k},\omega)] = Z_w(\underset{\sim}{k},\omega) = (\rho c / \bar{k}_z) ;$$

$$k_z = (\omega / c)\bar{k}_z , \tag{8}$$

where (c) is the speed of sound in the fluid, $(\underset{\sim}{k})$ is the wave vector variable in the plane of the boundary; $\underset{\sim}{k} = \{k_x, k_y\}$, and (ω) is the frequency variable. The wave equation in the fluid atop the boundary demands

$$\bar{k}_z = \bar{k}_3 ;$$
$$\bar{k}_3 = [1-(kc/\omega)^2]^{1/2} U\ [1-(kc/\omega)] - i[(kc/\omega)^2 - 1]^{1/2} U\ [(kc/\omega)-1] , \tag{9}$$

where

$$k^2 = |\underset{\sim}{k}|^2 = (k_x^2 + k_y^2) \ . \tag{10}$$

The incident pressure $P(\underset{\sim}{k},\omega)$ on the boundary is presented to the boundary as

$$P_b(\underset{\sim}{k},\omega) = P(\underset{\sim}{k},\omega)\ [1+R_p(\underset{\sim}{k},\omega)] \ , \tag{11}$$

where $R_p(\underset{\sim}{k},\omega)$ is the reflection coefficient of the boundary

$$R_p(\underset{\sim}{k},\omega) = [Z_p(\underset{\sim}{k},\omega) - Z_w(\underset{\sim}{k},\omega)]\ [Z_p(\underset{\sim}{k},\omega + Z_w(\underset{\sim}{k},\omega)]^{-1} \ , \tag{12}$$

and $Z_p(\underset{\sim}{k},\omega)$ is the mechanical surface impedance of the boundary; e.g., for a boundary that is equivalently a thin isotropic plate responding in flexure

$$Z_p(\underset{\sim}{k},\omega) = i\omega m\ [1-(k/k_p)^4\ (1+i\eta_p)] \ , \tag{13}$$

with

$$k_p^2 = [\omega\omega_c / c^2] \ . \tag{14}$$

In Eqs. (12) - (14), (m) is the mass per unit area, (k_p) is the flexural wavenumber and (η_p) is the loss factor in the boundary. Note that the flexural wavenumber (k_p) is defined in terms of the critical frequency (ω_c). From Eqs. (13) and (14) one obtains

$$Z_p(\underset{\sim}{k},\omega) = i\omega m\ [1-(kc/\omega)^4\ (\omega/\omega_c)^2\ (1+i\eta_p)] \ . \tag{15}$$

In Eq. (12) the surface impedance $Z_w(\underset{\sim}{k},\omega)$ is that of the fluid in the plane of the boundary . [cf. Eq. (8).] The factor $[1+R_p(\underset{\sim}{k},\omega)]$ is the "conditioning plate" filtering function; the filtering efficiency $C_p(\underset{\sim}{k},\omega)$ of the conditioning plate is then given by

$$C_p(\underset{\sim}{k},\omega) \;=\; |1+R_p(\underset{\sim}{k},\omega)|^2 = 4\;|Z_p(\underset{\sim}{k},\omega)|^2\;\;|Z_p(\underset{\sim}{k},\omega)+Z_\omega(\underset{\sim}{k},\omega)|^{-2}\;\;. \quad (16)$$

Equation (16) can be cast in the more explicit form

$$C_p(\underset{\sim}{k},\omega)=4\;\{\overline{C}_p(\underset{\sim}{k},\omega)\;\;U[1-(kc/\omega)] + \;\underline{C}_p(\underset{\sim}{k},\omega)\;\;U\{(kc/\omega)-1]\}\;\;, \quad (17)$$

where

$$\overline{C}_p=(C_{0p}/C_{1p})\;; \qquad \underline{C}_p \;=\; (C_{0p}/C_{2p})\;, \quad (18)$$

$$C_{0p} \;=\; [(1-\zeta)^2+(\eta_p\zeta)^2]\;; \qquad \zeta \;=\; (kc/\omega)^4(\omega/\omega_c)^2\;, \quad (19a)$$

$$(C_{1p})^{-1} \;=\; [1-(kc/\omega)^2]\;[\{1-(kc/\omega)^2\}(1-\zeta)^2$$

$$+\;\{\beta+[1-(kc/\omega)^2]^{1/2}(\eta_p\zeta)\}^2]^{-1}\;, \quad (19b)$$

$$(C_{2p})^{-1}=[(kc/\omega)^2-1]\;[\{\beta+[(kc/\omega)^2-1]^{1/2}(1-\zeta)\}^2$$

$$+\;\{(kc/\omega)^2-1]\}\;(\eta_p\zeta)^2]^{-1}\;, \quad (19c)$$

and the fluid loading ratio (β) and the fluid loading parameter (ε_c) are defined in the forms

$$\beta = (\rho c / \omega m) = (\omega_c / \omega)\varepsilon_c \; ; \qquad \varepsilon_c = (\rho c / \omega_c m) \; . \tag{20}$$

The filtering efficiency $C_p(\underset{\sim}{k},\omega)$ of the pressure conditioning plate is computed and depicted, as a function of (kc/ω), for a few representative parametric values, in Fig. 3. In particular, for the parametric values for which (β) and $(\zeta) <<< 1$, the filtering efficiency of the conditioning plate is simply a factor of (4), indicating a pressure doubling of the incident pressure at the boundary. This case is commensurate with a rigid boundary condition and is substantially depicted in Fig. 3 by the solid curve. Except in the close vicinity and at the sonic region, where $(kc/\omega) \approx 1$, the mechanical surface impedance $Z_p(\underset{\sim}{k},\omega)$ dominates the fluid surface impedance $Z_w(\underset{\sim}{k},\omega)$ and pressure doubling prevails, not only in the supersonic range but also in the covered subsonic range.

The short dashed curve in Fig. 3 depicts the case of

$$\beta = (\omega_c / \omega)\varepsilon_c \; ; \quad \varepsilon_c = 10^{-2} \text{ and } (\omega_c / \omega) = 10^2 \; ; \quad \eta_p = 10^{-2} \; . \tag{21a}$$

It is noted that in this case the frequency (ω) lies below the critical frequency and an anti-resonance, followed closely by a resonance, appears in the subsonic range. This doublet, however, is confined to a narrow span in the (kc/ω) range. Beyond the region of the doublet the pressure doubling is restored; the mechanical surface impedance, however, is now stiffness controlled rather than mass controlled. Indeed, it is the surface stiffness of the plate and the surface mass of the fluid that compose the dynamic system that resonates at $(kc/\omega) \simeq 10$. At this resonance $C_p(\underset{\sim}{k},\omega)$ is peaked; a peaked ridge in the filtering efficiency, in the subsonic range, is always detrimental, especially if the peak coincides with a densely populated region of noise components. The anti-resonance has the converse

effect. Awareness of the doublet and its features need to be kept in mind when designing a conditioning plate, however, within the context of a practical conditioning plate, these features are usually only of minor significance. Compared with the case in which (β) and $(\zeta) <<< 1$, as exhibited by the solid curve in Fig. 3, the case specified in Eq. (21a), as exhibited by the short dashed curve in Fig. 3, one observes that in front of the doublet, the "sonic deep" in the filtering efficiency remains, but is wider and the pressure doubling is weakened. This weakness in the boundary conditioning extends not only over the subsonic range, but more significantly into the supersonic range. Again, the doublet is significant only if it lies in the regional vicinity of major noise components.

The long dashed curve in Fig. 3 depicts the case of

$$\beta = (\omega_c / \omega)\varepsilon_c \; ; \quad \varepsilon_c = 10^{-1} \text{ and } (\omega_c / \omega) = 10 \; ; \quad \eta_p = 10^{-2} \; . \tag{21b}$$

This case is similar to that stated in Eq. (21a) and, therefore, the features of the short and the long dashed curves in Fig. 3 are similar too. There are, however, quantitative differences; e.g. in this case the dynamic system resonates at $(kc / \omega) \simeq (10)^{1/2}$ rather than at 10. There are also quantitative commonalities; e.g., the fluid loading ratio (β) in the parametric specifications in Eqs. (21a) and (21b) are identical.

Since the subsonic components in the incident pressure on the boundary are contributing, by definition, to the noise only, a device that diminishes these components from reaching the surfaces of the transducers is desirable. However, a device of this kind must not effect the supersonic components. The signal is contributed, by definition, of supersonic components only. Therefore, any diminishing of the filtering efficiency in the supersonic range is considered detrimental. A suitable device of this kind is the blanket. The filtering efficiency $B(\underset{\sim}{k}, \omega)$ of the blanket is of the form

$$B(\underset{\sim}{k},\omega) =$$

$$U[1-(kc/\omega)] + \exp[-2(b\omega/c)\{(kc/\omega)^2-1\}^{1/2}]\, U\{(kc/\omega)-1\} \quad , \quad (22)$$

where (b) is the thickness of the blanket. The filtering efficiency $B(\underset{\sim}{k},\omega)$ of the blanket, as a function of (kc/ω), for a few representatives parametric values is depicted in Fig. 4. In Fig. 4 the values of $(b\omega/c)$ are selected to be $(1/100)$, $(1/30)$, and $(2/30)$, respectively; for the first value the curve is solid, for the second it is a short dashed curve and for the third it is a long dashed curve.

The passive filtering efficiency $D_p(\underset{\sim}{k},\omega)$ for the pressure array is the combined passive filtering efficiency $C_p(\underset{\sim}{k},\omega)$ of the conditioning plate and the passive filtering efficiency $B(\underset{\sim}{k},\omega)$ of the blanket; namely

$$D_p(\underset{\sim}{k},\omega) = C_p(\underset{\sim}{k},\omega)\ B(\underset{\sim}{k},\omega) \ . \quad (23)$$

The passive filtering efficiency $D_p(\underset{\sim}{k},\omega)$ for a pressure array, as function of (kc/ω), for a few representative parametric values is depicted in Fig. 5. In Fig. 5 the value of the normalized thickness of the blanket is fixed at $(b\omega/c) = (1/30)$. The significant advantage of employing a blanket in the passive filtering efficiency is clearly demonstrated in comparing Figs. 3 and 5, notwithstanding that a blanket has the additional significance in that it introduces an increase in mechanical damping. This property of the blanket is not discussed herein because the type of responses that are especially influenced by this increase in damping are not considered in this primitive dissertation [13].

Designating $A_p(\underset{\sim}{k}_s \mid \underset{\sim}{k},\omega)$ the active filtering efficiency of the pressure array, the output $O_p(\underset{\sim}{k}_s,\omega)$ of this array to a pressure incident spectral density $\Phi_p(\underset{\sim}{k},\omega)$ is given by

$$O_p(\underset{\sim}{k}_s,\omega) \;=\; \int d\underset{\sim}{k}\;\; J_p(\underset{\sim}{k}_s \mid \underset{\sim}{k},\omega)\;\; \Phi_p(\underset{\sim}{k},\omega) \;\;;$$

$$J_p(\underset{\sim}{k}_s \mid \underset{\sim}{k},\omega) \;=\; A_p(\underset{\sim}{k}_s \mid \underset{\sim}{k},\omega)\;\; D_p(\underset{\sim}{k},\omega)\;, \tag{24}$$

where $J_p(\underset{\sim}{k}_s \mid \underset{\sim}{k},\omega)$ is the combined filtering efficiency of the pressure array.

II. PASSIVE FILTERING EFFICIENCY FOR A VELOCITY ARRAY

In analogy to Eq. (24), designating $A_v^o(\underset{\sim}{k}_s \mid \underset{\sim}{k},\omega)$ the active filtering efficiency and $D_v^o(\underset{\sim}{k},\omega)$ the passive filtering efficiency of a velocity array that is subjected to a velocity incident spectral density $\Phi_v(\underset{\sim}{k},\omega)$, the output of this array may be expressed in the form

$$O_v(\underset{\sim}{k}_s,\omega) = \int d\underset{\sim}{k}\ J_v^o(\underset{\sim}{k}_s \mid \underset{\sim}{k},\omega)\ \Phi_v(\underset{\sim}{k},\omega)\ ;$$

$$J_v^o(\underset{\sim}{k}_s \mid \underset{\sim}{k},\omega) = A^o(\underset{\sim}{k}_s \mid \underset{\sim}{k},\omega)\ D_v^o(\underset{\sim}{k},\omega)\ , \tag{25a}$$

where $J_v^o(\underset{\sim}{k}_s \mid \underset{\sim}{k},\omega)$ is the combined filtering efficiency of the velocity array. From Eq. (8) one establishes the relationship, between the pressure spectral density $\Phi_p(\underset{\sim}{k},\omega)$ and the velocity spectral density $\Phi_v(\underset{\sim}{k},\omega)$, to be

$$\Phi_v(\underset{\sim}{k},\omega) = |1-(kc/\omega)^2|(\rho c)^{-2}\Phi_p(\underset{\sim}{k},\omega)\ , \tag{26}$$

where (ρc) is the characteristic impedance of the fluid. Substituting Eq. (26) in Eq. (25a) one may cast the output $O_v(\underset{\sim}{k}_s,\omega)$ of the velocity array, to a pressure incident spectral density $\Phi_p(\underset{\sim}{k},\omega)$, in the form

$$O_v(\underset{\sim}{k}_s,\omega) = \int d\underset{\sim}{k}\ J_v(\underset{\sim}{k}_s \mid \underset{\sim}{k},\omega)\ \Phi_p(\underset{\sim}{k},\omega)\ ;$$

$$J_v(\underset{\sim}{k}_s \mid \underset{\sim}{k},\omega) = A_v(\underset{\sim}{k}_s \mid \underset{\sim}{k},\omega)\ D_v(\underset{\sim}{k},\omega)\ , \tag{25b}$$

where

$$A_v(\underset{\sim}{k}_s \mid \underset{\sim}{k},\omega) \;=\; [A_v^o(\underset{\sim}{k}_s \mid \underset{\sim}{k},\omega)/(\rho c)^2] \;; \qquad D_v(\underset{\sim}{k},\omega) \;=\; D_v^o(\underset{\sim}{k},\omega)\;\; E_p^v(\underset{\sim}{k},\omega) \;;$$

$$E_p^v(\underset{\sim}{k},\omega) \;=\; |1-(kc/\omega)^2| \;. \tag{27a}$$

The factor $E_p^v(\underset{\sim}{k},\omega)$ is dubbed the **conversion** filtering efficiency.

The active filtering efficiency $A_v(\underset{\sim}{k}_s \mid \underset{\sim}{k},\omega)$ of a velocity array is tacitly assumed to be similar to that of the active filtering efficiency $A_p(\underset{\sim}{k}_s \mid \underset{\sim}{k},\omega)$ of a pressure array. In this event one may state

$$A_p(\underset{\sim}{k}_s \mid \underset{\sim}{k},\omega) \;\equiv\; A_v(\underset{\sim}{k}_s \mid \underset{\sim}{k},\omega) \;=\; [A_v^o(\underset{\sim}{k}_s \mid \underset{\sim}{k},\omega)/(\rho c)^2] \;. \tag{27b}$$

The active filtering efficiency in both, the pressure array and the velocity array, as stated in Eq. (27), is steered to the wave vector $(\underset{\sim}{k}_s)$ on the boundary. [cf. Eq. (2).]

The leading filtering efficiency factor $B(\underset{\sim}{k},\omega)$ in the passive filtering efficiency $D_v(\underset{\sim}{k},\omega)$ is that of the blanket. This filtering efficiency factor is stated in Eq. (22) and is featured in Fig. 4. The next filtering efficiency factor in $D_v(\underset{\sim}{k},\omega)$ is that of the conversion from pressure to velocity spectral density; that factor is designated $E_p^v(\underset{\sim}{k},\omega)$ and is explicitly stated in Eq. (27a). The conversion filtering efficiency $E_p^v(\underset{\sim}{k},\omega)$, as a function of (kc/ω), is depicted in Fig. 6a. The "superdirectivity" of this filtering efficiency in the supersonic range is clearly discernible in this figure. This superdirectivity culminates with the sharp valley and nadir in the vicinity and at the sonic region where $(kc/\omega) \;\approx\; 1$. On the other hand, in the subsonic range, past the brief remainder of the sonic valley that is associated with the superdirectivity, the conversion filtering efficiency favors accepting the

higher and higher subsonic components at the quadratic rate of $(kc/\omega)^2$. As explained, such an increase in the filtering efficiency is detrimental to the signal-to-noise maximization desired in the performance of the array. The blanket appears to be a promising antidote for the kind of deficiency in the conversion filtering efficiency $E_p^{\nu}(\underset{\sim}{k},\omega)$ that is exhibited in Fig. 6a. Figure 6b depicts the combined filtering efficiency $[E_p^{\nu}(\underset{\sim}{k},\omega)\ \ B(\underset{\sim}{k},\omega)]$, as a function of (kc/ω), for the three normalized thicknesses used in Fig. 4; i.e., $(b\omega/c) = (1/100), (1/30)$ and $(2/30)$. The relief that is provided by the blankets in mitigating the acceptance at the higher and higher ranges of (kc/ω) is clearly visible in Fig. 6b when compared with Fig. 6a. Finally, an observation is made with respect to the conversion filtering efficiency $E_p^{\nu}(\underset{\sim}{k},\omega)$. Clearly, Eq. (25a) may be cast in the form

$$O_{\nu}(\underset{\sim}{k}_s,\omega) = \int d\underset{\sim}{k}\ \ J'_{\nu}(\underset{\sim}{k}_s \mid \underset{\sim}{k},\omega)\ \ \Phi_p(\underset{\sim}{k},\omega)\ ;$$

$$J'_{\nu}(\underset{\sim}{k}_s \mid \underset{\sim}{k},\omega) = A'_{\nu}(\underset{\sim}{k}_s \mid \underset{\sim}{k},\omega)\ \ D'_{\nu}(\underset{\sim}{k},\omega)\ , \tag{25c}$$

where

$$A'_{\nu}(\underset{\sim}{k}_s \mid \underset{\sim}{k},\omega) = E_p^{\nu}(\underset{\sim}{k},\omega)\ \ A_{\nu}(\underset{\sim}{k}_s \mid \underset{\sim}{k},\omega)\ ;$$

$$J'_{\nu}(\underset{\sim}{k}_s \mid \underset{\sim}{k},\omega) = J_{\nu}(\underset{\sim}{k}_s \mid \underset{\sim}{k},\omega) = A_{\nu}(\underset{\sim}{k}_s \mid \underset{\sim}{k},\omega)\ \ D_{\nu}(\underset{\sim}{k},\omega)\ . \tag{28}$$

The shifting of the conversion filtering efficiency $E_p^{\nu}(\underset{\sim}{k},\omega)$, from the passive to the active filtering efficiency, as stated in Eq. (25c), makes the designation of superdirectivity in the active filtering efficiency easier to understand. In the passive filtering efficiency $D_{\nu}(\underset{\sim}{k},\omega)$, the interpretation of the conversion filtering efficiency $E_p^{\nu}(\underset{\sim}{k},\omega)$ is straightforward but it

does not readily connote the notion of superdirectivity. Nonetheless, for the most part in this report the conversion filtering efficiency is placed with the passive filtering efficiency.

The final filtering efficiency factor in $D_v(\underset{\sim}{k},\omega)$ is that of the conditioning of the boundary. The conversion of the spectral density from a pressure to a velocity necessitates that the conditioning of a boundary be maximized for velocity spectral components. The incident velocity $V(\underset{\sim}{k},\omega)$ on the boundary is presented as

$$V_b(\underset{\sim}{k},\omega) \;=\; V(\underset{\sim}{k},\omega)\,[1+R_v(\underset{\sim}{k},\omega)]\;, \tag{29}$$

where $R_v(\underset{\sim}{k},\omega)$ is the reflection coefficient of the boundary

$$\begin{aligned} R_v(\underset{\sim}{k},\omega) \;&=\; -R_p(\underset{\sim}{k},\omega) \\ &=\; [Z_w(\underset{\sim}{k},\omega) - Z_p(\underset{\sim}{k},\omega)]\,[Z_w(\underset{\sim}{k},\omega) + Z_p(\underset{\sim}{k},\omega)]^{-1}\;, \end{aligned} \tag{30}$$

and again, $Z_p(\underset{\sim}{k},\omega)$ is the mechanical surface impedance the boundary, which for the velocity array is selected to be compliant; e.g.,

$$Z_p(\underset{\sim}{k},\omega) \;=\; (K/i\omega)\;\;;\;\; K \;=\; K_o(1+i\eta_o)\;, \tag{31}$$

where it is customary, but not necessary, to regard (K_o) a constant, independent of $(\underset{\sim}{k})$ and (ω). [cf. Eqs. (11) - (15).] The factor $[1+R_v(\underset{\sim}{k},\omega)]$ is the conditioning compliance filtering function; the filtering efficiency $C_v(\underset{\sim}{k},\omega)$ of the conditioning compliance is given by

$$\begin{aligned} C_v(\underset{\sim}{k},\omega) \;&=\; |1-R_p(\underset{\sim}{k},\omega)|^2 \\ &=\; 4\,|Z_w(\underset{\sim}{k},\omega)|^2\;\;|Z_p(\underset{\sim}{k},\omega) + Z_w(\underset{\sim}{k},\omega)|^{-2}\;. \end{aligned} \tag{32}$$

[cf. Eq. (16).] Equation (32) may be cast in the more explicit form

$$C_v(\underset{\sim}{k},\omega) = 4\{\overline{C}_v(\underset{\sim}{k},\omega)\ U\ [1-(kc/\omega)]$$

$$+\ \underline{C}_v(\underset{\sim}{k},\omega)\ U[(kc/\omega)-1]\}\ , \tag{33}$$

where

$$\overline{C}_v = (C_{1v})^{-1}\ ; \qquad \underline{C}_v = (C_{2v})^{-1}\ , \tag{34}$$

$$C_{1v} = [\{1+[1-(kc/\omega)^2]^{1/2}\ (\eta_o\beta_o)\}^2 + [1-(kc/\omega)^2]\ \beta_o^2]\ , \tag{35a}$$

$$C_{2v} = [\{1-[(kc/\omega)^2-1]^{1/2}\beta_o\}^2 + [(kc/\omega)^2-1](\eta_o\beta_o)^2]\ , \tag{35b}$$

and the "inverse fluid loading ratio" (β_o) and the "inverse fluid loading parameter" (ε_o) are defined in the forms·

$$\beta_o = [K_o/(\omega\rho c)] = (\omega_o/\omega)\varepsilon_o\ ; \qquad \varepsilon_o = [K_o/(\omega_o\rho c)]\ . \tag{36}$$

[cf. Eq. (20).] The filtering efficiency $C_v(\underset{\sim}{k},\omega)$ of the velocity conditioning compliance, as a function of (kc/ω), is depicted in Fig. 7. In particular, for the parametric value for which $\beta_o <<< 1$, the filtering efficiency of the conditioning compliance is simply a factor of (4), indicating a velocity doubling of the incident velocity at the boundary. This case is commensurate with a "pressure release boundary condition" and is substantially depicted in Fig. 7 by the solid curve. The surface compliance (the inverse of the surface stiffness) is

low enough that the pressure release condition is maintained throughout the covered range of (kc/ω); both the supersonic and the subsonic ranges are so maintained.

The short dashed curve in Fig. 7 depicts the case of

$$\beta_o = (\omega_o/\omega)\varepsilon_o \; ; \; \varepsilon_o = 10^{-2} \text{ and } (\omega_o/\omega) = 10 \; ; \; \eta_o = 10^{-1} \; . \quad (37a)$$

Equation (35b) suggests that for a value of (β_o) that is small, but not very small, compared with unity a resonance, in the covered subsonic range, results. The resonance occurs in the dynamic system that is composed of the surface stiffness of the boundary and the fluid surface mass on the plane of the boundary. For the parametric values specified in Eq. (37a), the resonance is located at $(kc/\omega) \simeq 10$. Below the resonance, where $(kc/\omega) < 10$, the pressure release condition substantially prevails, the more so the further (kc/ω) is away from the resonance at $(kc/\omega) \simeq 10$. Above the resonance, where $(kc/\omega) > 10$, the surface stiffness effectively increases, as (kc/ω) further increases, and the pressure release condition is greatly departed from. In that subsonic range, the departure reduces the acceptance of the filtering efficiency $C_\nu(k,\omega)$ inversely to the increase in the conversion filtering efficiency $E_p^\nu(\underset{\sim}{k},\omega)$. That subsonic range is defined by $(kc/\omega) > 10$, which lies above the resonance at $(kc/\omega) \simeq 10$. This latter feature is depicted in Fig. 8 by the short dashed curve. In this figure the combined passive filtering efficiency $D_{1\nu}(\underset{\sim}{k},\omega)$ is displayed, as a function of (kc/ω), for a set of parametric values that correspond to those specified for Fig. 7. The combined passive filtering efficiency $D_{1\nu}(\underset{\sim}{k},\omega)$ is defined as the product of the conversion filtering efficiency $E_p^\nu(\underset{\sim}{k},\omega)$ and the filtering efficiency $C_\nu(\underset{\sim}{k},\omega)$ of the compliantly conditioned boundary; namely

$$D_{1\nu}(\underset{\sim}{k},\omega) = C_\nu(\underset{\sim}{k},\omega)E_p^\nu(\underset{\sim}{k},\omega) \; . \quad (38)$$

The short dashed curve in Fig. 8, which correspondingly is specified in Eq. (37a), supports the conjuncture just made with respect to the range above the resonance: In the subsonic range above the resonance, where $(kc/\omega) > 10$, the quadratic increase in $E_p^{\nu}(\underset{\sim}{k},\omega)$ is counteracted by the quadratic decrease in $C_p(\underset{\sim}{k},\omega)$. The quadratic increase and decrease are in reference to the normalized wavenumber (kc/ω).

The long dashed curve in Fig. 7 depicts the case of

$$\beta_o = (\omega_o/\omega)\varepsilon_o \; ; \quad \varepsilon_o = 10^{-1} \text{ and } (\omega_o/\omega) = 10 \; ; \quad \eta_o = 10^{-1} \; . \qquad (37b)$$

For the parametric values specified in Eq. (37b) the resonance is located just above the sonic region, which is defined by $(kc/\omega) = 1$. Below the resonance, where $(kc/\omega) < 1$, the pressure release condition tends, but "half" fails, to be established; the mechanical surface impedance which is stiffness controlled, is too high to maintain a substantially pressure release condition. Above the resonance, where $(kc/\omega) >> 1$, the surface stiffness effectively increases, as (kc/ω) further increases, and the pressure release condition is greatly departed from. Again, in the subsonic range this departure reduces the acceptance of the filtering efficiency $C_{\nu}(\underset{\sim}{k},\omega)$. In the subsonic range past the resonance location, this reduction in acceptance is inversely proportional to the increase in the conversion filtering efficiency $E_p^{\nu}(\underset{\sim}{k},\omega)$. Again, this feature is depicted in Fig. 8 by the long dashed curve; this curve depicts $D_{1\nu}(\underset{\sim}{k},\omega)$, as a function of (kc/ω), for the parametric values specified in Eq. (37b). The combined filtering efficiency $D_{1\nu}(\underset{\sim}{k},\omega)$ is as stated in Eq. (38).

One recognizes that in this report the passive filtering efficiency $D_{1\nu}(\underset{\sim}{k},\omega)$ is the **basic** passive filtering efficiency of the velocity array. Therefore, Fig. 8 is more relevant to a design process of a velocity array, than is Fig. 7. From Fig. 8 it emerges that, barring densely populated subsonic components in the close vicinity of the sonic region, the parametric values specified in Eq. (37b) are more suitable to achieving a well designed

velocity array. More suitable than those specified in Eq. (37a) and by far more suitable than those maintaining the "ideal pressure release condition." This statement holds despite the existence of a slight deterioration (by a factor of half) in the supersonic range, where $(kc/\omega) < 1$, when the parametric values specified in Eq. (37b) are implemented. The closer the resonance is to the sonic region, where $(kc/\omega) \simeq 1$, the better the filtering efficiency $C_v(\underset{\sim}{k},\omega)$ of the conditioning compliance is able to counteract the detrimental quadratic increase of the acceptance in the conversion filtering efficiency $E_p^v(\underset{\sim}{k},\omega)$ in the higher-subsonic range. Indeed, except for the doublet in Fig. 3 and the resonance in Fig. 8, the parametric specification in Eq. (21) for the pressure array yields filtering efficiency that is closely identified with the filtering efficiency for a velocity array under the parametric specifications in Eq. (37b). However, before rendering such a comparison one may wish to examine the utility of a blanket on the passive filtering efficiency of a velocity array.

The blanket introduces the factor $B(\underset{\sim}{k},\omega)$ in the passive filtering efficiency $D_v(\underset{\sim}{k},\omega)$ of the velocity array. From Eqs. (22) and (38) one obtains

$$D_v(\underset{\sim}{k},\omega) = D_{1v}(\underset{\sim}{k},\omega)\ B(\underset{\sim}{k},\omega)\ . \tag{39}$$

The filtering efficiency $B(\underset{\sim}{k},\omega)$ of a blanket is depicted in Fig. 4. The introduction of a blanket, of a normalized thickness of $(b\omega/c) = (1/30)$, on a boundary, as specified in Eq. (39), is computed and depicted, as a function of (kc/ω), in Fig. 9. The benefit to the filtering efficiency derived from the introduction of a blanket is clearly visible in comparing Figs. 8 and 9. Again, the superiority of a design employing the parametric specification in Eq. (37b), over that specified in Eq. (37a) and that specified by the ideal pressure release condition, is made clearer in Fig. 9. This is especially true if the spectral noise components are similar to those proposed in Fig. 1. In this connection it may of interest to examine Fig. 6b in the light of Fig. 9. In Fig. 6b, one recalls, the ideal pressure release boundary is maintained throughout the covered spectral range of (kc/ω) and various normalized

thicknesses for the blanket are introduced on this ideal pressure release boundary. The relevant curve in Fig. 9 pertains to a blanket of a normalized thickness $(b\omega/c)$ of $(1/30)$, as well as to the parametric specification in Eq. (37b). Comparing this curve in Fig. 9 with the curve in Fig. 6b, which pertains to a boundary of ideal pressure release condition covered by a blanket of double the thickness; i.e., a normalized thickness $(b\omega/c)$ of $(2/30)$, one finds that the identity between the two curves, in the respective figures, is reasonably close. One must be cognizant, however, that a pressure release boundary may be influenced unduly when subjected to changes in the prevailing hydrostatic pressure. The hydrostatic pressure may drastically change from one array operation to another.

A more comprehensive examination of this and other statements made in the attempt to compare the pressure and velocity arrays follows.

III. COMPARISON BETWEEN PRESSURE AND VELOCITY ARRAYS

In this comparison the identify stated in Eq. (27b) is validated. In this case the output $O_p(\underset{\sim}{k}_s,\omega)$ of the pressure array may be expressed in the form

$$O_p(\underset{\sim}{k}_s,\omega) \;=\; \int d\underset{\sim}{k}\;\; A_p(\underset{\sim}{k}_s\,|\,\underset{\sim}{k},\omega)\;\; D_p(\underset{\sim}{k},\omega)\;\; \Phi_p(\underset{\sim}{k},\omega)\;, \tag{40a}$$

and the output $O_v(\underset{\sim}{k}_s,\omega)$ of the velocity array may be expressed in the form

$$O_v(\underset{\sim}{k}_s,\omega) \;=\; \int d\underset{\sim}{k}\;\; A_p(\underset{\sim}{k}_s\,|\,\underset{\sim}{k},\omega)\;\; D_v(\underset{\sim}{k},\omega)\;\; \Phi_p(\underset{\sim}{k},\omega)\;, \tag{40b}$$

where the passive filtering efficiencies of the respective arrays are

$$D_p(\underset{\sim}{k},\omega) \;=\; C_p(\underset{\sim}{k},\omega)\;\; B(\underset{\sim}{k},\omega)\;, \tag{41a}$$

$$D_v(\underset{\sim}{k},\omega) \;=\; D_{1v}(\underset{\sim}{k},\omega)\;\; B(\underset{\sim}{k},\omega)\;;\quad D_{1v}(\underset{\sim}{k},\omega) \;=\; C_v(\underset{\sim}{k},\omega)\;\; E_p^v(\underset{\sim}{k},\omega)\;. \tag{41b}$$

[cf. Eqs. (24) and (25).] Following the suggestion proposed in Eq. (1), it is proposed to cast the incident pressure spectral density in the form

$$\Phi_p(\underset{\sim}{k},\omega) \;=\; \Phi_{pS}(\underset{\sim}{k}_s,\omega)\;\; \delta(\underset{\sim}{k}_s-\underset{\sim}{k}) \;+\; \Phi_{pN}(\underset{\sim}{k},\omega)\;;$$

$$\delta(\underset{\sim}{k}_s-\underset{\sim}{k}) \;\equiv\; \delta(k_{sx}-k_x)\;\; \delta(k_{sy}-k_y)\;;\qquad \underset{\sim}{k}_s \;=\; \{k_{sx},k_{sy}\}\;. \tag{42}$$

In Eq. (42) the first term in the first equation accounts for the incident spectral density of the signal, the second term accounts for the incident spectral density of the noise. From Eqs. (4), (40) and (42) one derives for the signal outputs

$$O_{pS}(\underset{\sim}{k}_s,\omega) = A_p(\underset{\sim}{k}_s \mid \underset{\sim}{k}_s,\omega)\ D_p(\underset{\sim}{k}_s,\omega)\ \Phi_{pS}(\underset{\sim}{k}_s,\omega)\ , \tag{43a}$$

$$O_{vS}(\underset{\sim}{k}_s,\omega) = A_p(\underset{\sim}{k}_s \mid \underset{\sim}{k}_s,\omega)\ D_v(\underset{\sim}{k}_s,\omega)\ \Phi_{pS}(\underset{\sim}{k}_s,\omega)\ , \tag{43b}$$

and, by definition, $(\underset{\sim}{k}_s)$ is supersonic in the sense that $(\mid \underset{\sim}{k}_s \mid c/\omega) < 1$. From Eqs. (4), (40) and (42) one obtains for the noise outputs

$$O_{pN}(\underset{\sim}{k}_s,\omega) = \int d\underset{\sim}{k}\ J_p(\underset{\sim}{k}_s \mid \underset{\sim}{k},\omega)\ \Phi_{pN}(\underset{\sim}{k},\omega)\ , \tag{44a}$$

$$O_{vN}(\underset{\sim}{k}_s,\omega) = \int d\underset{\sim}{k}\ J_p(\underset{\sim}{k}_s \mid \underset{\sim}{k},\omega)\ \Phi_{vN}(\underset{\sim}{k},\omega)\ , \tag{44b}$$

where

$$J_p(\underset{\sim}{k}_s \mid \underset{\sim}{k},\omega) = A_p(\underset{\sim}{k}_s \mid \underset{\sim}{k},\omega)\ D_p(\underset{\sim}{k},\omega)\ , \tag{45a}$$

$$\Phi_{vN}(\underset{\sim}{k},\omega) = T_p^v(\underset{\sim}{k},\omega)\ \Phi_{pN}(\underset{\sim}{k},\omega)\ ;$$

$$T_p^v(\underset{\sim}{k},\omega) = [D_{1v}(\underset{\sim}{k},\omega)/C_p(\underset{\sim}{k},\omega)]\ , \tag{45b}$$

and $D_p(\underset{\sim}{k},\omega)$, $C_p(\underset{\sim}{k},\omega)$ and $D_{1v}(\underset{\sim}{k},\omega)$ are defined in Eqs. (23), (16) and (38), respectively. The quantity $\Phi_{vN}(\underset{\sim}{k},\omega)$ is the **effective** spectral density of the incident pressure on the boundary that is presented to the filtering efficiency of an equivalent

pressure array. An equivalent pressure array is a velocity array in which the combined filtering efficiency is made to conform with that of a corresponding bonafide pressure array. The differences in the outputs of the two arrays are then assigned to the incident spectral densities that they, respectively, need to cope with. Thus, the output $O_{vN}(\underset{\sim}{k}_s, \omega)$ of the velocity array differs from the output $O_{pN}(\underset{\sim}{k}_s, \omega)$ of the pressure array in that the former equivalently copes with the incident spectral density $\Phi_{vN}(\underset{\sim}{k}, \omega)$ whereas the latter correspondingly copes with the incident spectral density $\Phi_{pN}(\underset{\sim}{k}, \omega)$. In this sense $T_p^v(\underset{\sim}{k}, \omega)$ facilitates the spectral amplification factor for the noise spectral density; in those spectral ranges in which $T_p^v(\underset{\sim}{k}, \omega)$ exceeds unity, the contribution by the incident spectral density $\Phi_{pN}(\underset{\sim}{k}, \omega)$ to $O_{vN}(\underset{\sim}{k}_s, \omega)$ exceeds that to $O_{pN}(\underset{\sim}{k}_s, \omega)$ and in those ranges in which $T_p^v(\underset{\sim}{k}, \omega)$ recedes unity, this contribution to $O_{vN}(\underset{\sim}{k}_s, \omega)$ recedes that to $O_{pN}(\underset{\sim}{k}_s, \omega)$. Thus, if, on balance, the factor $T_p^v(\underset{\sim}{k}, \omega)$ contributes more into $O_{vN}(\underset{\sim}{k}_s, \omega)$ than it substracts from it, the noise output $O_{vN}(\underset{\sim}{k}_s, \omega)$ in the velocity array exceeds the noise output $O_{pN}(\underset{\sim}{k}_s, \omega)$ in the pressure array.

The signal-to-noise ratios R_{pN}^S and R_{vN}^S à la Eq. (3) is given by

$$R_{pN}^S(\underset{\sim}{k}_s, \omega) = [O_{pS}(\underset{\sim}{k}_s, \omega) / O_{pN}(\underset{\sim}{k}_s, \omega)] , \tag{46a}$$

for the pressure array and

$$R_{vN}^S(\underset{\sim}{k}_s, \omega) = [O_{vS}(\underset{\sim}{k}_s, \omega) / O_{vN}(\underset{\sim}{k}_s, \omega)] , \tag{46b}$$

for the velocity array, respectively. The advantage or disadvantage of the pressure array over the velocity array may be ascertained by estimating the "grand ratio" of the signal-to-noise ratios of the pressure and velocity arrays. This grand ratio $R_v^p(\underset{\sim}{k}_s, \omega)$ is given by

$$R_v^p(\underset{\sim}{k}_s,\omega) \;=\; [R_{pN}^S(\underset{\sim}{k}_s,\omega)/R_{vN}^S(\underset{\sim}{k}_s,\omega)] \;. \tag{48}$$

A value of $R_v^p(\underset{\sim}{k}_s,\omega)$ that largely exceeds unity implies that the pressure array is superior, on the basis of signal-to-noise ratio, to the velocity array and a value of $R_v^p(\underset{\sim}{k}_s,\omega)$ that largely recedes unity implies the superiority of the velocity array over the pressure array. From Eqs. (43) - (47) the grand ratio $R_v^p(\underset{\sim}{k}_s,\omega)$ may be cast in the form

$$R_v^p(\underset{\sim}{k}_s,\omega) \;=\; [T_p^v(\underset{\sim}{k}_s,\omega)]^{-1}\;[O_{vN}(\underset{\sim}{k}_s,\omega)/O_{pN}(\underset{\sim}{k}_s,\omega)] \;, \tag{49}$$

where $(\underset{\sim}{k}_s)$ is, by definition, a supersonic wave vector; i.e., $(|(\underset{\sim}{k}_s|c/\omega) \;<\; 1$ and $T_p^v(\underset{\sim}{k},\omega)$, $O_{pN}(\underset{\sim}{k}_s,\omega)$ and $O_{vN}(\underset{\sim}{k}_s,\omega)$ are defined in Eqs. (45b), (44a) and (44b), respectively. The evaluations of the last two quantities; $O_{pN}(\underset{\sim}{k}_s,\omega)$ and $O_{vN}(\underset{\sim}{k}_s,\omega)$, require the execution of integrations over known incident spectral densities. Although such integrations were previously performed and these types of integrations can be presently duplicated, there is a merit in trying to estimate these quantities without actually executing the integrations. The technique to be followed concentrates on the nature of the integrads and assesses the major contributions that various regions in the $(kc/\omega)-$domain may be bringing into the outputs of the arrays. The orders of magnitude and the regions from which these contributions may emanate are of crucial interest in seeking initial design criteria for these two characteristic arrays. For this purpose the incident spectral density $\Phi_{pN}(\underset{\sim}{k},\omega)$ is assumed to possess a term $\Phi_{TBL}(\underset{\sim}{k},\omega)$ that is commensurate with that generated on a boundary by a turbulent boundary layer (TBL). The investigation in this report is driven by $\Phi_{TBL}(\underset{\sim}{k},\omega)$ which serves as the dominant term in the spectral density $\Phi_{pN}(\underset{\sim}{k},\omega)$ of the noise incident on the boundary.

IV. A RUDIMENTARY DESCRIPTION OF THE SPECTRAL DENSITY OF THE PRESSURE GENERATED BY A TURBULENT BOUNDARY LAYER (TBL)

For the purposes of this report the incident spectral density $\Phi_{pN}(\underset{\sim}{k},\omega)$ of the noise is assumed to be dominated largely by the pressure that is generated by TBL. A rudimentary description of that spectral density is

$$\Phi_{pN}(\underset{\sim}{k},\omega) \simeq \Phi_{TBL}(\underset{\sim}{k},\omega) = [\Phi_{nx}(k_x,\omega) + \Phi_{cx}(k_x,\omega)]\ \Phi_{ny}(k_y,\omega)\ , \quad (49)$$

where

$$\Phi_{nx}(k_x,\omega) = a[\alpha^2 + (1+|(k_x c/\omega)M_c|)^2]^{-1}\ , \quad (50a)$$

$$\Phi_{ny}(k_y,\omega) = \beta^2[\beta^2 + (k_y c/\omega)^2 M_c^2]^{-1}\ , \quad (50b)$$

$$\Phi_{cx}(k_x,\omega) = \{[\alpha^2 + (1-[(k_x c/\omega)M_c])^2]^{-1} - [\alpha^2 + (1+|(k_x c/\omega)M_c|)^2]^{-1}\}\ , \quad (50c)$$

where $\alpha \simeq 0.1$, $\beta = 3\alpha$ and M_c is the Mach number of the convective speed (U_c) with respect to the speed of sound (c) in the fluid. Plots of $\Phi_{TBL}(k_x,0,\omega)$ as a function of $(k_x c/\omega)$ and of $\Phi_{TBL}(k_y,0,\omega)$ as a function of $(k_y c/\omega)$ are presented in Fig. 10 for values of the constant $a = 1, 10^{-1}$ and 10^{-2}. The non-isotropic nature of the spectral density $\Phi_{TBL}(\underset{\sim}{k},\omega)$ is discernible; the convective ridge results in that most components in a TBL tend to assume the wave vector that is commensurate with the convective velocity $\underset{\sim}{U}_c = \{U_c,0\}$. Elsewhere in the spectral domain on the boundary, the TBL components are sparsed. It is understood that the convective Mach number M_c;

$M_c = (U_c / c)$, is usually small in arrays that are intended to be used in underwater application. The convective wavenumber is thus high compared with the sonic wavenumber and, therefore, the convective ridge lies in the high-subsonic region. For convective speeds of 20 knots, M_c is two orders of magnitude small. Therefore, even a blanket of reasonable thickness is a very effective inhibitor of the convective ridge. Indeed, the blanket can prevent the convective ridge from overwhelming the noise contribution to the output $O_{pN}(\underset{\sim}{k}_s, \omega)$. As to whether a well designed pressure array that is reasonably blanketed can render the convective ridge irrelevant as a noise contributor is not yet resolved. There is still a controversy with regard to the distribution of the population of the spectral component outside the convective ridge in the spectral density of TBL, notwithstanding that, in addition, the high wavenumber response of the conditioning plate is not properly accounted for. Indeed, this controversy is reflective of the triple designation for the constant (a), stated in Eq. (50a) and depicted in Fig. 10.

In this paper computed estimations that pertain to a TBL are depicted for the situation in which the convective Mach number M_c is two orders of magnitude small; namely, $M_c = 10^{-2}$. In the primitive analysis developed herein reasonable changes in M_c are readily implemented. Moreover, the modifications induced by these changes do not cause special interpretative difficulties.

V. THE GRAND RATIO OF A PRESSURE ARRAY TO A CORRESPONDING VELOCITY ARRAY

In view of Fig. 10, the output $O_{pN}(\underset{\sim}{k}_s, \omega)$ is roughly and conveniently approximated in the form of four terms

$$O_{pN}(\underset{\sim}{k}_s, \omega) = O_{pN1}(\underset{\sim}{k}_s, \omega) + O_{pN2}(\underset{\sim}{k}_s, \omega) + O_{pN3}(\underset{\sim}{k}_s, \omega) + O_{pN4}(\underset{\sim}{k}_s, \omega) , \quad (51a)$$

where the first term is contributed by the TBL into the supersonic range, the second by the TBL into the low-subsonic range, the third by the TBL into the mid-subsonic range and the fourth is contributed by the convective ridge of the TBL which lies, in the context of this report, at the high-subsonic range. Again, one is reminded that the steered wave vector $(\underset{\sim}{k}_s)$ lies in the supersonic range; $(|(\underset{\sim}{k}_s| c/\omega) < 1$. Again, which of the four terms in Eq. (51a) dominates the output $O_{pN}(\underset{\sim}{k}_s, \omega)$ is crucially dependent not only on the spectral density $\Phi_{TBL}(\underset{\sim}{k}, \omega)$ in the TBL, but also on the filtering efficiency $J_p(\underset{\sim}{k}_s | \underset{\sim}{k}, \omega)$ of the pressure array. This filtering efficiency is assumed to be designed to maximize the signal-to-noise ratio $R^S_{pN}(\underset{\sim}{k}_s, \omega)$, as stated in Eq. (46a). How does the estimate of the output $O_{pN}(\underset{\sim}{k}_s, \omega)$, as stated in Eq. (51a), help one to estimate the output $O_{vN}(\underset{\sim}{k}_s, \omega)$ and, hence, the signal-to-noise ratio $R^S_{vN}(\underset{\sim}{k}_s, \omega)$, as stated in Eq. (46b), and, ultimately, to estimate the grand ratio $R^p_v(\underset{\sim}{k}_s, \omega)$, as stated in Eq. (49)? To answer this question it may be useful to compute and display the natures of $T^v_p(\underset{\sim}{k}, \omega)$ and $\Phi_{vN}(\underset{\sim}{k}, \omega)$; the latter on the basis that $\Phi_{pN}(\underset{\sim}{k}, \omega)$ is substantially equal to $\Phi_{TBL}(\underset{\sim}{k}, \omega)$. The spectral density $\Phi_{TBL}(\underset{\sim}{k}, \omega)$ in a TBL is depicted in Fig. 10. In Fig. 11 the factor $T^v_p(\underset{\sim}{k}, \omega)$ is computed and displayed for a number of cases that are covered in Figs. 3-9. In Fig. 11a the nearly ideal rigid conditioning plate for the pressure array and the nearly ideal pressure release conditioning compliance are entered to yield the factor $T^v_p(\underset{\sim}{k}, \omega)$. The so called

"superdirectivity" is discernible in the vicinity and on both sides of the sonic region. Also discernible is the quadratic increase in (kc/ω) of $T_p^v(\underset{\sim}{k},\omega)$ in the higher-subsonic range; e.g. $T_p^v(\underset{\sim}{k},\omega) \simeq 10^4$ when $(kc/\omega) \simeq 10^2$. The corresponding increase in the spectral density $\Phi_{vN}(\underset{\sim}{k},\omega)$ over that of $\Phi_{pN}(\underset{\sim}{k},\omega)$ is depicted in Fig. 12a. The corresponding situation for the cross-convective domain is depicted in Fig. 12.1a. Therefore, in the subsonic range the velocity array is equivalently subjected to a higher incident spectral density than is the pressure array; the equivalence is as expressed in Eqs. (44) and (45). Figure 12a indicates that the increase of $\Phi_{vN}(\underset{\sim}{k},\omega)$ over $\Phi_{pN}(\underset{\sim}{k},\omega)$, in the convective ridge, is a whopping 40 dB, or so, for the convective Mach number M_c of 10^{-2}. The convective ridge may then become a major noise source for a velocity array even if a pressure array successfully mitigates the contribution by this convective ridge. The equivalent pressure array, which simulates the velocity array, needs to deal with the convective ridge in $\Phi_{vN}(\underset{\sim}{k},\omega)$. The bonafide pressure array needs merely deal with the convective ridge in $\Phi_{pN}(\underset{\sim}{k},\omega)$.

When a resonance in the compliantly conditioned boundary occurs in the subsonic range below the convective ridge, the situation is improved, as shown in Figs. 11b and 11c and 12b and 12c, respectively. Figure 12.1c depicts the corresponding cross-convective domain to Fig. 12.1c. In Figs. 11b and 12b this resonance is substantially coincidental with the doublet that occurs in the conditioning plate for the pressure array. As already discussed, the resonance in the compliantly conditioned boundary mollifies the increase in the acceptance that is introduced by the conversion filtering efficiency $E_p^v(\underset{\sim}{k},\omega)$ that the velocity array entertains. This mollification halves, in dB, the enhancement in these figures as compared with that shown in Figs. 11a and 12a. Nonetheless, the enhancement is still forbiddingly high. Moreover, in the lower-subsonic range there is a gain of an order of magnitude in these figures over the levels shown in Figs. 11a and 12a. Although in the lower-subsonic range the spectral density $\Phi_{TBL}(\underset{\sim}{k},\omega)$ is small compared with that in the convective ridge, both the blanket and the array shading are less effective in this lower-

subsonic range than in the higher-subsonic range, and therefore, this gain cannot be dismissed off hand in a design process.

When the resonance in the compliantly conditioned boundary approaches the sonic region, the situation is improved still, as shown in Figs. 11d and 11e and 12d and 12e, respectively. The corresponding situation in the cross-convective domain to Fig. 12e is depicted in Fig. 12.1e. This resonance in the conditioning compliance substantially eliminates the increase in the acceptance that is introduced by the conversion filtering efficiency $E_p^v(\underset{\sim}{k},\omega)$ that the velocity array harbors. The factor $T_p^v(\underset{\sim}{k},\omega)$ is different from unity only in the region of the resonance. In this case, the resonance occupies a narrow subsonic region next to the sonic region and in the immediate vicinity of the same region. Again, although in this narrow subsonic region the spectral density $\Phi_{TBL}(\underset{\sim}{k},\omega)$ is small compared with that in the convective ridge, the filtering efficiency of the pressure array may not be as effective in this subsonic range as it may be at the higher-subsonic range. Therefore, even a moderate gain in $\Phi_{vN}(\underset{\sim}{k},\omega)$, as compared with $\Phi_{pN}(\underset{\sim}{k},\omega)$, in this narrow subsonic region, as just described, cannot be cavalierly dismissed in a design process, notwithstanding that the doublet in the conditioning plate is usually ignored.

With these observations on hand and noting that $T_p^v(\underset{\sim}{k},\omega)$, as stated herein, is isotropic, the output $O_{vN}(\underset{\sim}{k}_s,\omega)$ may be expressed à la Eq. (51a) in the approximate form

$$O_{vN}(\underset{\sim}{k}_s,\omega) \simeq T_p^v(\underset{\sim}{k}_s,\omega)\ O_{pN1}(\underset{\sim}{k}_s,\omega) + T_p^v(\underset{\sim}{k}_2,\omega)\ O_{pN2}(\underset{\sim}{k}_s,\omega)$$

$$+ T_p^v(\underset{\sim}{k}_3,\omega)\ O_{pN3}(\underset{\sim}{k}_s,\omega) + T_p^v(\underset{\sim}{k}_4,\omega)\ O_{pN4}(\underset{\sim}{k}_s,\omega)\ , \qquad (51b)$$

where $(|(\underset{\sim}{k}_s|c/\omega)<1;\ \ 1<(|(\underset{\sim}{k}_2|c/\omega)<10;\ \ 10<(|(\underset{\sim}{k}_3|c/\omega)\simeq 10^2;$ $(|(\underset{\sim}{k}_4|c/\omega)\simeq (M_c)^{-1}$, and the values of T_p^v, at the wave vectors $\underset{\sim}{k}_2$, $\underset{\sim}{k}_3$ and $\underset{\sim}{k}_4$, are derived on the basis of applying, in unison, primitive mean value approximations to the

two equations covered in Eq. (44). Applying the case depicted in Figs. 11a and 12a to Eq. (51b) yields

$$O_{vN}(\underset{\sim}{k}_s,\omega) \simeq O_{pN1}(\underset{\sim}{k}_s,\omega) + 10^1\ O_{pN2}(\underset{\sim}{k}_s,\omega)$$

$$+ 10^2\ O_{pN3}(\underset{\sim}{k},\omega) + 10^4\ O_{pN4}(\underset{\sim}{k}_s,\omega) . \qquad (52a)$$

Applying the case depicted in Figs. 11b and 11c and 12b and 12c to Eq. (51b) yields

$$O_{vN}(\underset{\sim}{k}_s,\omega) \simeq 2\ O_{pN1}(\underset{\sim}{k}_s,\omega) + 10^2\ O_{pN2}(\underset{\sim}{k}_s,\omega)$$

$$+ 10^2\ O_{pN3}(\underset{\sim}{k},\omega) + 10^2\ O_{pN4}(\underset{\sim}{k}_s,\omega) . \qquad (52b)$$

Finally, applying the case depicted in Figs. 11d and 11e and 12d and 12e to Eq. (51b) yields

$$O_{vN}(\underset{\sim}{k}_s,\omega) \simeq O_{pN1}(\underset{\sim}{k}_s,\omega) + 10\ O_{pN2}(\underset{\sim}{k}_s,\omega)$$

$$+ O_{pN3}(\underset{\sim}{k}_s,\omega) + O_{pN4}(\underset{\sim}{k}_s,\omega) . \qquad (52c)$$

Using Eqs. (48) and (51a), the corresponding grand ratios $R_v^p(\underset{\sim}{k}_s,\omega)$ for the three cases depicted in Eq. (52), assume the estimated values

$$R_v^p(\underset{\sim}{k}_s,\omega) =$$
$$[O_{pN1}(\underset{\sim}{k}_s,\omega) + 10^1\ O_{pN2}(\underset{\sim}{k}_s,\omega) + 10^2\ O_{pN3}(\underset{\sim}{k}_s,\omega) + 10^4\ O_{pN4}(\underset{\sim}{k}_s,\omega)]$$

$$[O_{pN1}(\underset{\sim}{k}_s,\omega) + O_{pN2}(\underset{\sim}{k}_s,\omega) + O_{pN3}(\underset{\sim}{k}_s,\omega) + O_{pN4}(\underset{\sim}{k}_s,\omega)]^{-1} , \qquad (53a)$$

$$R_v^p(\underset{\sim}{k}_s,\omega) =$$

$$[O_{pN1}(\underset{\sim}{k}_s,\omega) + 5\text{x}10^1\ O_{pN2}(\underset{\sim}{k}_s,\omega) + 5\text{x}10^1\ O_{pN3}(\underset{\sim}{k}_s,\omega) + 5\text{x}10^1\ O_{pN4}(\underset{\sim}{k}_s,\omega)]$$

$$[O_{pN1}(\underset{\sim}{k}_s,\omega) + O_{pN2}(\underset{\sim}{k}_s,\omega) + O_{pN3}(\underset{\sim}{k}_s,\omega) + O_{pN4}(\underset{\sim}{k}_s,\omega)]^{-1} \ . \qquad (53b)$$

and

$$R_v^p(\underset{\sim}{k}_s,\omega) =$$

$$[O_{pN1}(\underset{\sim}{k}_s,\omega) + 10\ O_{pN2}(\underset{\sim}{k}_s,\omega) + O_{pN3}(\underset{\sim}{k}_s,\omega) + O_{pN4}(\underset{\sim}{k}_s,\omega)]$$

$$[O_{pN1}(\underset{\sim}{k}_s,\omega) + O_{pN2}(\underset{\sim}{k}_s,\omega) + O_{pN3}(\underset{\sim}{k}_s,\omega) + O_{pN4}(\underset{\sim}{k}_s,\omega)]^{-1} \ , \qquad (53c)$$

respectively. The relative magnitudes among the terms of Eq. (51a) are crucial to the estimation of the grand ratio $R_v^p(\underset{\sim}{k}_s,\omega)$. Equation (53) indicates, however, that for the three cases here considered the grand ratio $R_v^p(\underset{\sim}{k}_s,\omega)$ invariably exceeds unity and, therefore, assessed by the signal-to-noise ratios, the pressure array is advantaged over the corresponding velocity array. The question that remains is by how much? Again, Eq. (53) may be used to assess the quantitative advantage. Thus, for example, if the convective ridge is the dominant contributor to the output $O_{pN}(\underset{\sim}{k}_s,\omega)$; i.e., if $O_{pN4}(\underset{\sim}{k}_s,\omega)$ is the dominant term in $O_{pN}(\underset{\sim}{k}_s,\omega)$ of Eq. (51a), then from Eqs. (53a) - (53c) one may deduce

$$R_v^p(\underset{\sim}{k}_s,\omega) \simeq 10^4 \ , \qquad (54a)$$

$$R_v^p(\underset{\sim}{k}_s,\omega) \simeq 50 \ , \qquad (54b)$$

and

$$R_v^p(\underset{\sim}{k}_s,\omega) \simeq \{1 + 10[O_{pN2}(\underset{\sim}{k}_s,\omega)/O_{pN4}(\underset{\sim}{k}_s,\omega)]\} ;$$

$$[O_{pN2}(\underset{\sim}{k}_s,\omega)/O_{pN4}(\underset{\sim}{k}_s,\omega)] << 1 , \tag{54c}$$

respectively. On the other hand, again, as an example, if the low-subsonic range in the TBL is the dominant contributor to the output $O_{pN}(\underset{\sim}{k}_s,\omega)$, i.e., if $O_{pN2}(\underset{\sim}{k}_s,\omega)$ is the dominant term in $O_{pN}(\underset{\sim}{k}_s,\omega)$ of Eq. (51a), then from Eqs. (53a) - (53c) one may deduce that

$$R_v^p(\underset{\sim}{k}_s,\omega) \simeq$$
$$\{10 + 10^2\ [O_{pN3}(\underset{\sim}{k}_s,\omega)/O_{pN2}(\underset{\sim}{k}_s,\omega)] + 10^4\ [O_{pN4}(\underset{\sim}{k}_s,\omega)/O_{pN2}(\underset{\sim}{k}_s,\omega)]\} ;$$

$$[O_{pN3}(\underset{\sim}{k}_s,\omega)/O_{pN2}(\underset{\sim}{k}_s,\omega)] << 1 ; \quad O_{pN4}(\underset{\sim}{k}_s,\omega)/O_{pN2}(\underset{\sim}{k}_s,\omega)] << 1 , \tag{55a}$$

$$R_v^p(\underset{\sim}{k}_s,\omega) \simeq 50 , \tag{55b}$$

and

$$R_v^p(\underset{\sim}{k}_s,\omega) \simeq 10 , \tag{55c}$$

respectively. In both examples, in the third case, as stated in Eqs. (54c) and (55c), the pressure array is only marginally advantaged over the corresponding velocity array. Notwithstanding that in the first case, as stated in Eqs. (54a) and (55a), the advantage is substantially higher. Unfortunately, it is the first case that is usually cited and one then concludes that a corresponding velocity array, as far as the TBL is concerned, is a hopeless

proposition when compared with a bonafide pressure array. In this report it is argued that this conclusion may not be universally valid. Indeed, it is demonstrated that a properly designed conditioning compliance may render a corresponding velocity array a viable alternative to a pressure array if the noise is assumed to be contributed largely by TBL.

VI. A FEW DESIGN ISSUES

The analyses, the computations and the displays in this report are primitively based and omit many issues that may be crucial to the validity and universality of the statements and conclusions made. It is not intended to raise and discuss these issues exhaustively. It is intended to exemplify a few of these issues and to briefly indicate their implications.

1. The quantity $\Phi_{TBL}(\underset{\sim}{k},\omega)$ may not be the only incident noise component on the boundary. The response of substructures, either in the immediate spatial vicinity or as members of the arrays, may generate subsonic components that lie within an order of magnitude of the sonic region; e.g., analogous to the doublet in the response of the conditioning plate. [cf. Fig. 3.] Under these circumstances, the resonance near the sonic region, which is designed to counteract the quadratic increase with (kc/ω) of the conversion filtering efficiency $E_p^v(\underset{\sim}{k},\omega)$, may itself present a design problem.

2. The conditioned boundary in which the array is flush mounted may not be of uniform surface impedance. In the report, uniformity is assumed. Nonuniformity is a wave vector scattering mechanism which may redistribute, in particular, the noise components with high wavenumbers. The gaps and the isolators that are placed between transducers constitute such nonuniformities. The influence of the redistribution of the noise components which may be caused by such nonuniformities may require design considerations.

3. The surface of the array is not motionless; the boundary is convected with the velocity of the vehicle housing the array. If the blanket is placed on the boundary, this motion may trap propagating waves that lie close to the sonic region [14]. The trapping and the strengths of these propagating waves may be another candidate for design consideration.

4. The compliance in a boundary of a velocity array is usually provided by a matrix of voids in an elastic plating. Be that as it may, the voids provide a scattering mechanism;

that mechanism is especially effective when the voids linear spatial sizes become of the order of magnitude or larger than the linear spatial sizes of the waves in the incident pressure on the elastic plating. The introduction of a thick blanket, in terms of these wave sizes, may mitigate that scattering mechanism. This is especially significant if the components in the convective ridge of TBL are commensurate with these wave sizes. In this connection, the blanket may inhibit the scattering mechanisms that are provided by the nonuniformities discussed under remark 2. The thickness and material properties of the blanket are yet another design consideration that may need attention.

5. Considerations in this report are concentrated largely on a specific frequency (ω). For a narrow frequency band $(\Delta\omega)$ for which $(\Delta\omega / \omega)$ is small compared with unity, these considerations are adequately covered, even when resonances are invoked. However, if operations of the arrays are needed in wider frequency bands, more thorough assessments than those provided herein may be called upon in designing these wider frequency arrays. Nonetheless, it may be of interest to investigate cursorily this issue of a frequency bandwidth. In this vein estimates for the influence of changing the frequencies are computed and displayed in Fig. 13 in the format of Fig. 12. In Fig. 13 both (ω_o / ω) and (ω_c / ω) are equal and ε_o and ε_c are both set equal to 10^{-1}. As in Fig. 12, in Fig. 13 the incident spectral density of a TBL is depicted by a short dashed curve. This is the assumed spectral density of the noise that a bonafide pressure array needs to cope with. The solid curve in Fig. 13 represents the spectral density that an equivalent pressure array needs to cope with to simulate the noise output of a corresponding velocity array. In Figs. 13a-13i the frequency is changed so that $(\omega_o / \omega) = (\omega_c / \omega) = 20, 18, 16, 14, 12, 10, 8, 6$ and 4, respectively, yet (ε_o) and (ε_c) remain equal and set at 10^{-1}. It is recognized that Fig. 13f is identical to Fig. 12e. The advantages and disadvantages, that each of these figures exhibits with respect to a pressure and a velocity array, are explainable within the context of this report. Remarkably, over the frequency bandwidth of a octave up and an octave down from the frequency set in Figs. 12e and 13f; namely,

$(\omega_o / \omega) = (\omega_c / \omega) = 10$, the resonances in the compliantly conditioned boundary are maintaining a reasonable par between a bonafide pressure array and a corresponding velocity array. In these frequency range and parametric specifications, a bonafide pressure array and an equivalent pressure array need to cope, to all intents and purposes, with the same incident spectral density; i.e., $\Phi_{vN}(\underset{\sim}{k}, \omega) \simeq \Phi_{pN}(\underset{\sim}{k}, \omega)$ substantially over the entire (kc / ω) range. If any and as already mentioned, the closer the resonance frequency, in the compliantly conditioned fluid loaded boundary, is to the sonic region the more favor is accrued to the velocity array. This accrument does not, however, overwhelm the viability of the pressure array.

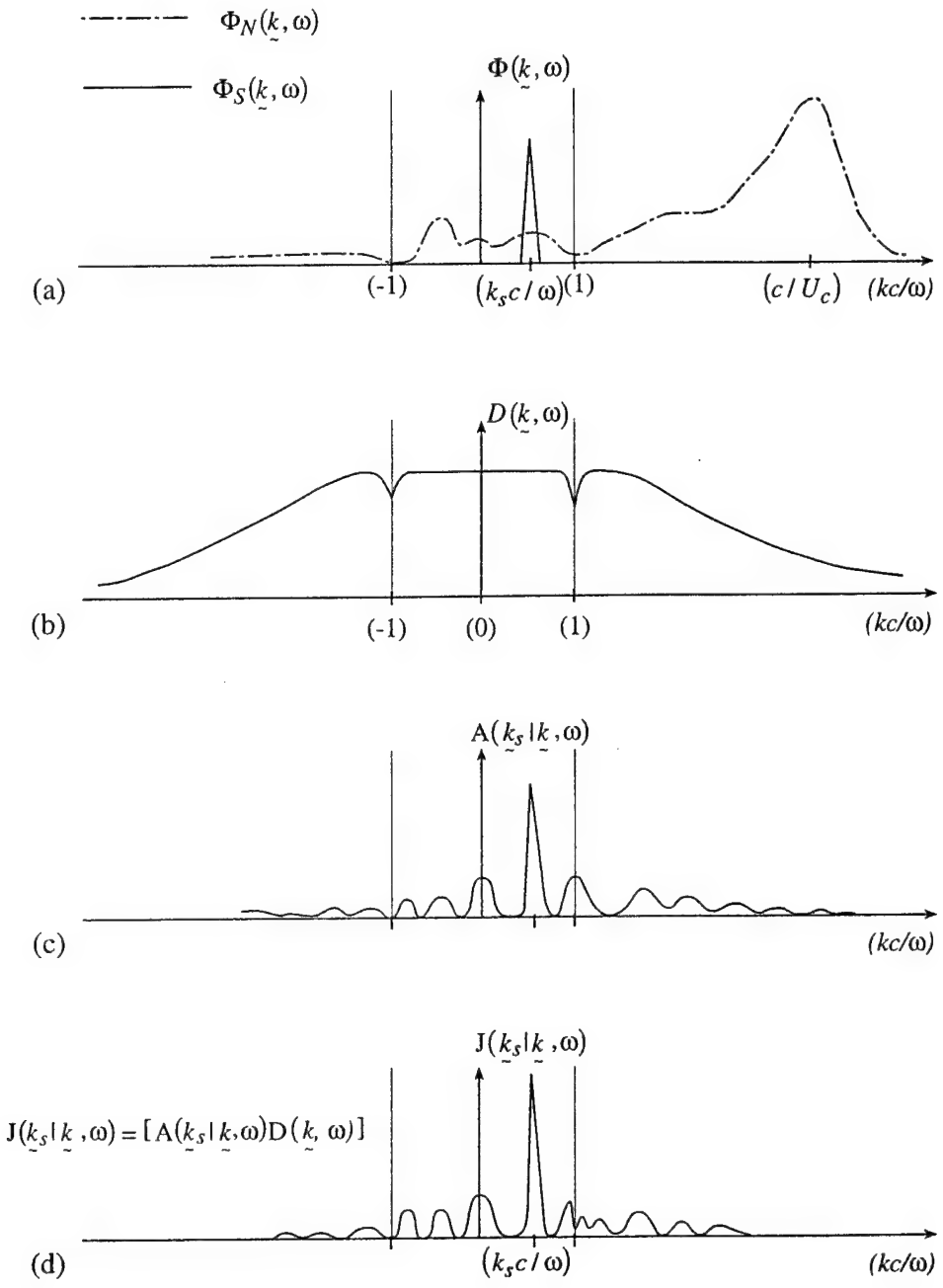

Fig. 1. The incident spectral densities of the signal and the noise and the filtering efficiencies of an array of transducers flush mounted in a plane boundary.

a. The spectral densities of the signal and the noise.

b. The passive filtering efficiency of the array.

c. The active filtering efficiency of the array.

d. The combined filtering efficiency of the array.

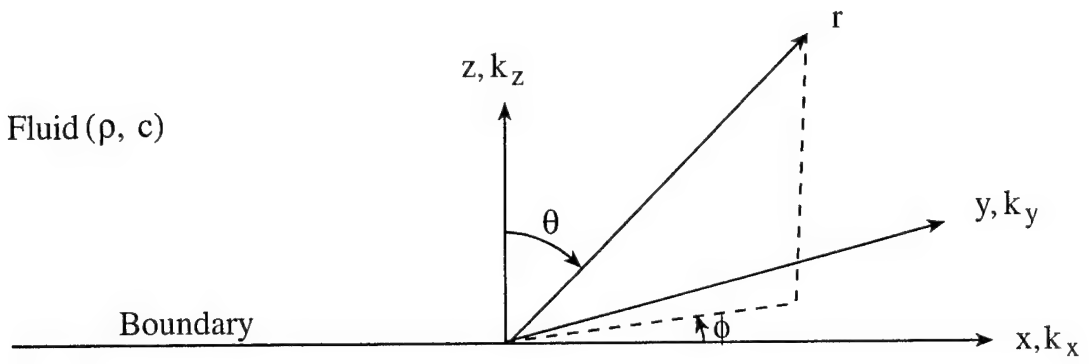

$$r^2 = x^2 + y^2 + z^2$$

$$x = r\,sin\,(\theta)\cos(\phi)$$
$$y = r\,sin\,(\theta) sin\,(\phi)$$
$$z = r\cos\,(\theta)$$

$$(\omega / c)^2 = k_x^2 + k_y^2 + k_z^2 ; k_z = k_3$$

$$\left.\begin{aligned} k_x &= (\omega / c) sin\,(\theta)\cos(\phi) \\ k_y &= (\omega / c)\, sin\,(\theta)\, sin(\phi) \\ k_3 &= (\omega / c)\cos(\theta) \end{aligned}\right\}, (kc / \omega) < 1$$

$$k_3 = -(i\omega / c)[(kc / \omega)^2 - 1]^{1/2}, (kc / \omega) > 1$$

Fig. 2. The plane boundary faced by a semi-infinite space filled with a fluid defined by the density (ρ) and speed of sound (c). Sketched is the coordinate system and briefly outlined are the relationships between the various variables in the spatial and spectral domains.

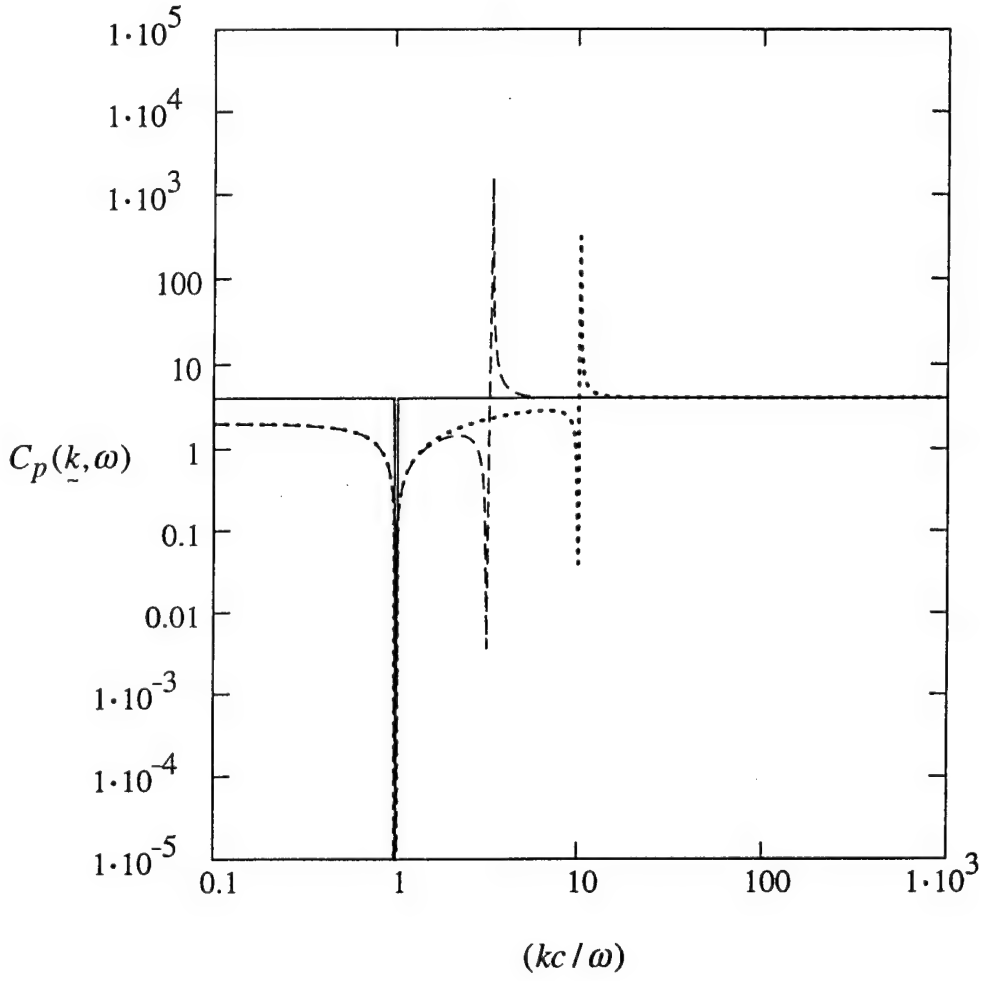

Fig. 3. The filtering efficiency $C_p(\underset{\sim}{k}, \omega)$ of the conditioning plate of a pressure array, as a function of (kc / ω).

—— An ideal conditioning plate [(β) and (ζ) <<< 1].

····· Parametric values specified in Eq. (21a).

– – – Parametric values specified in Eq. (21b).

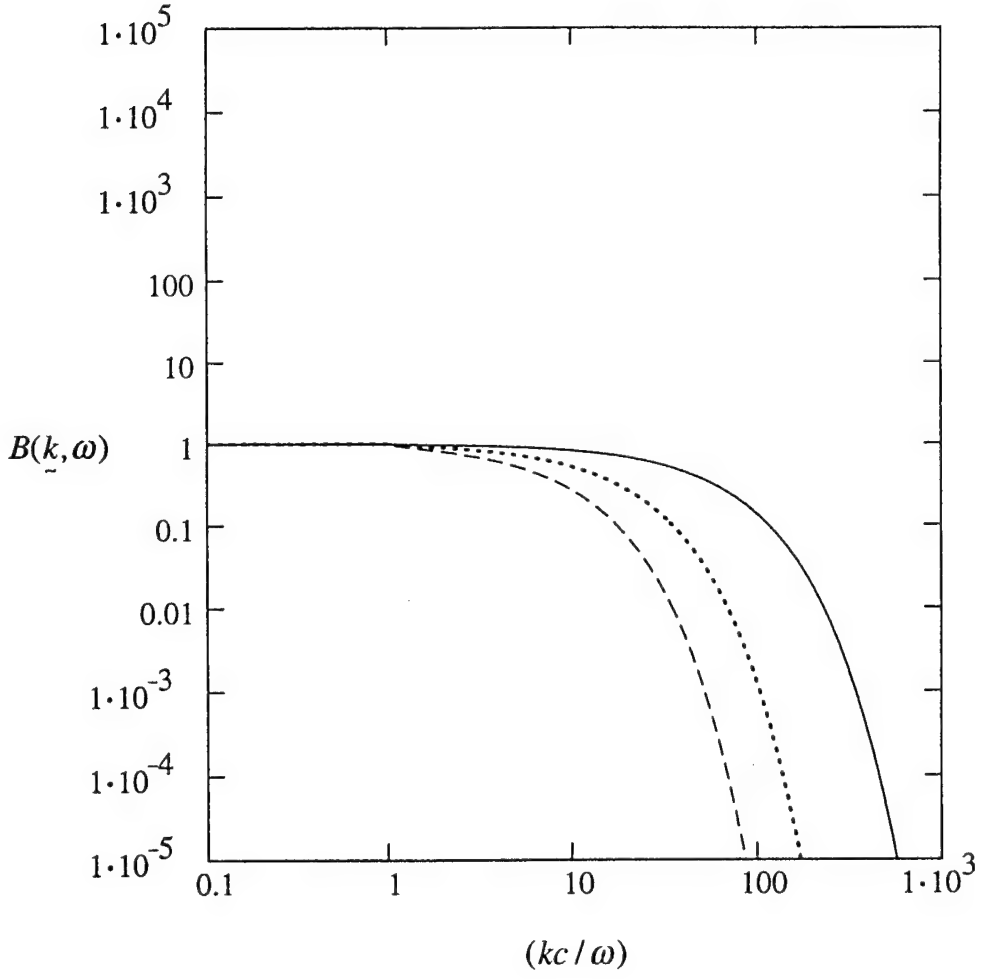

Fig. 4. The filtering efficiency $B(\underset{\sim}{k},\omega)$ of a blanket of thickness (b), as a function of (kc/ω).

—— $(b\omega/c) = (1/100)$.

····· $(b\omega/c) = (1/30)$.

– – – $(b\omega/c) = (2/30)$.

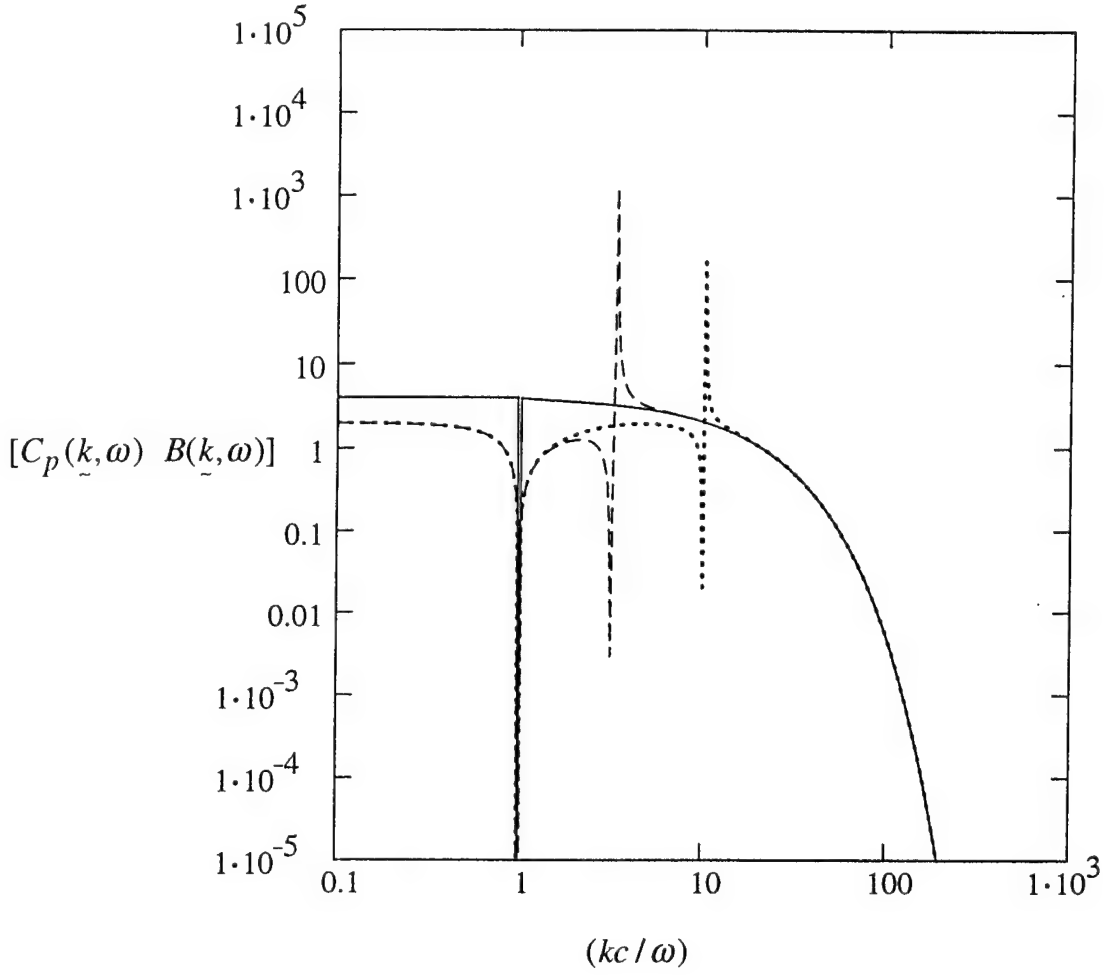

Fig. 5. The filtering efficiency $[C_p(\underset{\sim}{k},\omega)\ \ B(\underset{\sim}{k},\omega)]$ of a blanket conditioning plate, as a function of (kc/ω). The thickness of the blanket is $(b\omega/c) = (1/30)$.

—— An ideal conditioning plate [(β) and $(\zeta) <<< 1$].

····· Parametric values specified in Eq. (21a).

– – – Parametric values specified in Eq. (21b).

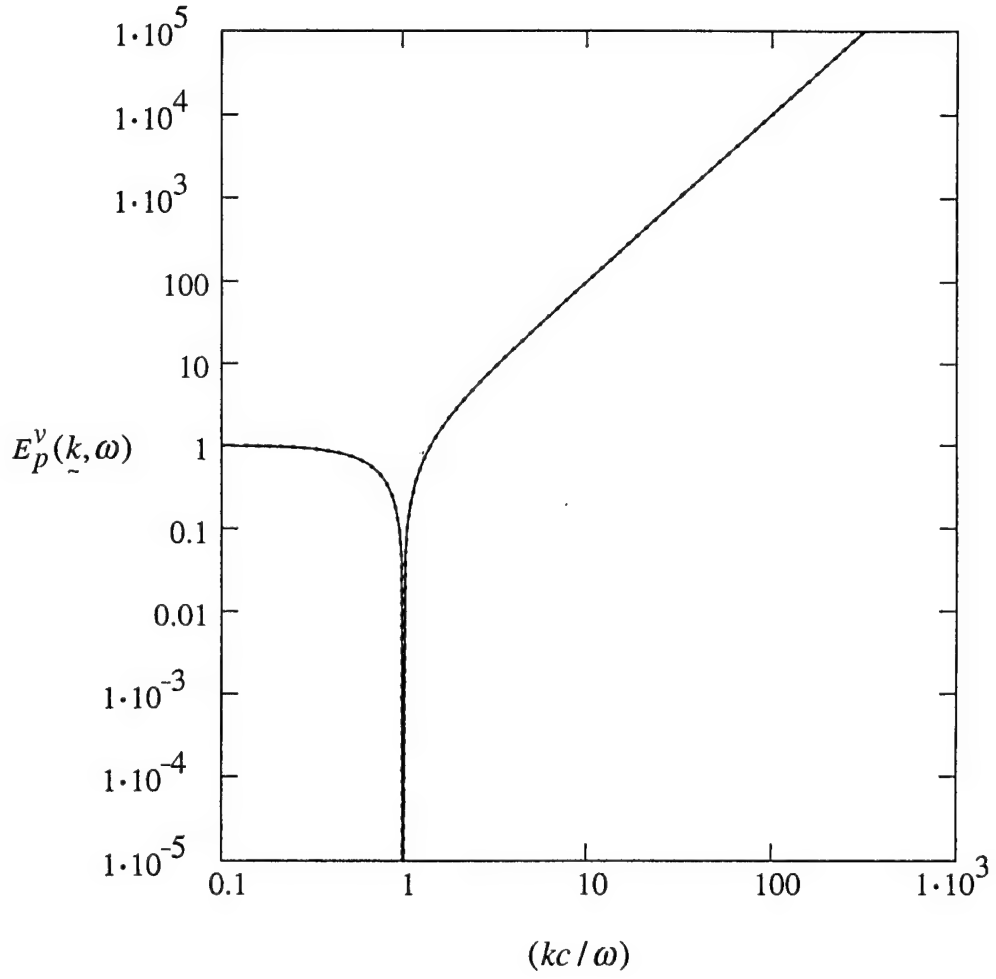

Fig. 6a. The conversion filtering efficiency $E_p^v(\underset{\sim}{k},\omega)$ as a function of (kc/ω).

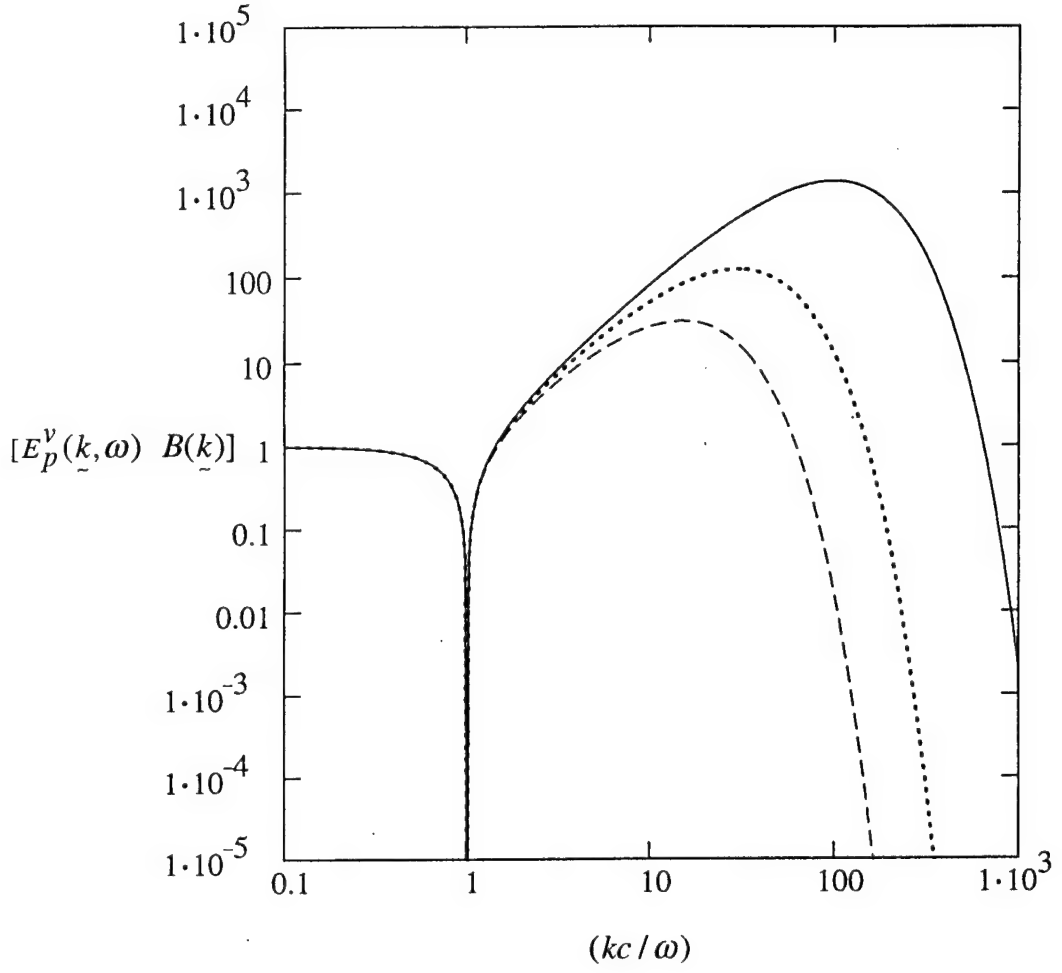

Fig. 6b. The filtering efficiency $[E_p^v(\underset{\sim}{k},\omega)\ \ B(\underset{\sim}{k})]$ of a blanketed conversion from pressure to velocity spectral density, as a function of (kc/ω).

—— $(b\omega/c) = (1/100)$.

····· $(b\omega/c) = (1/30)$.

– – – $(b\omega/c) = (2/30)$.

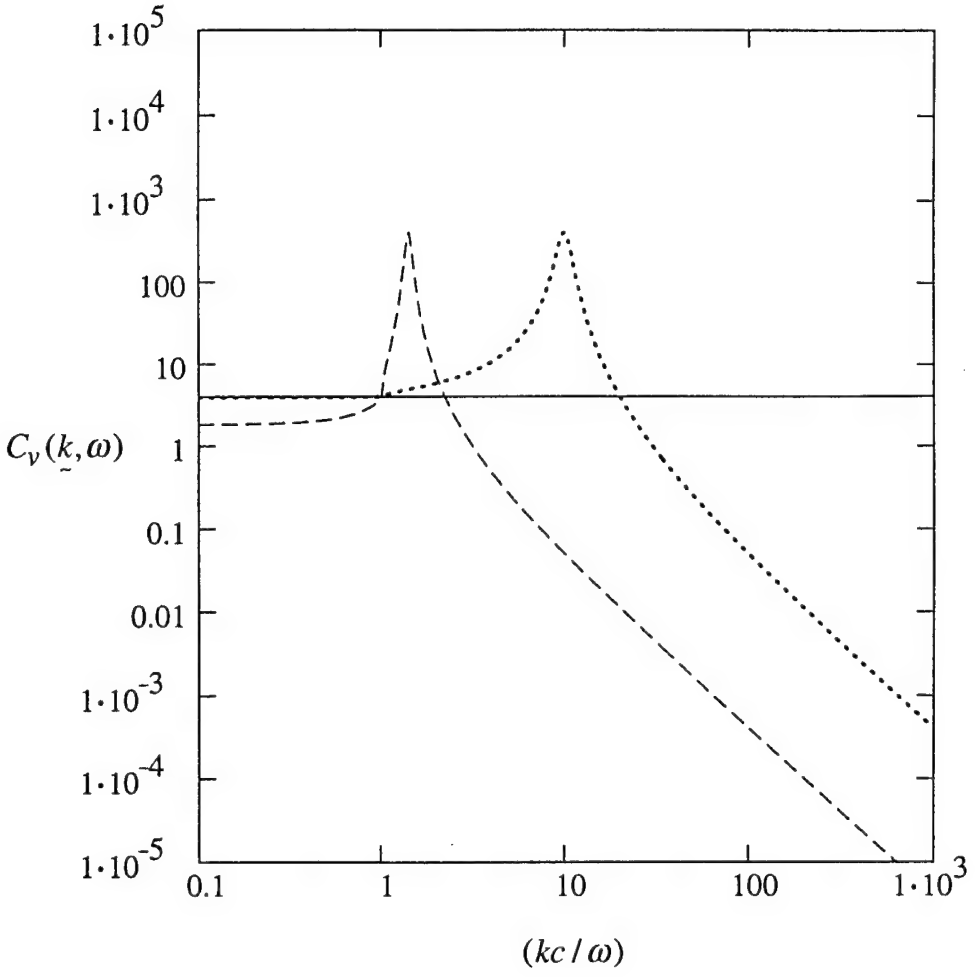

Fig. 7. The filtering efficiency $C_v(\underset{\sim}{k},\omega)$ of a compliantly conditioned boundary, as a function of (kc/ω).

—— An ideal pressure release condition [β_o <<< 1].

····· Parametric values specified in Eq. (37a).

– – – Parametric values specified in Eq. (37b).

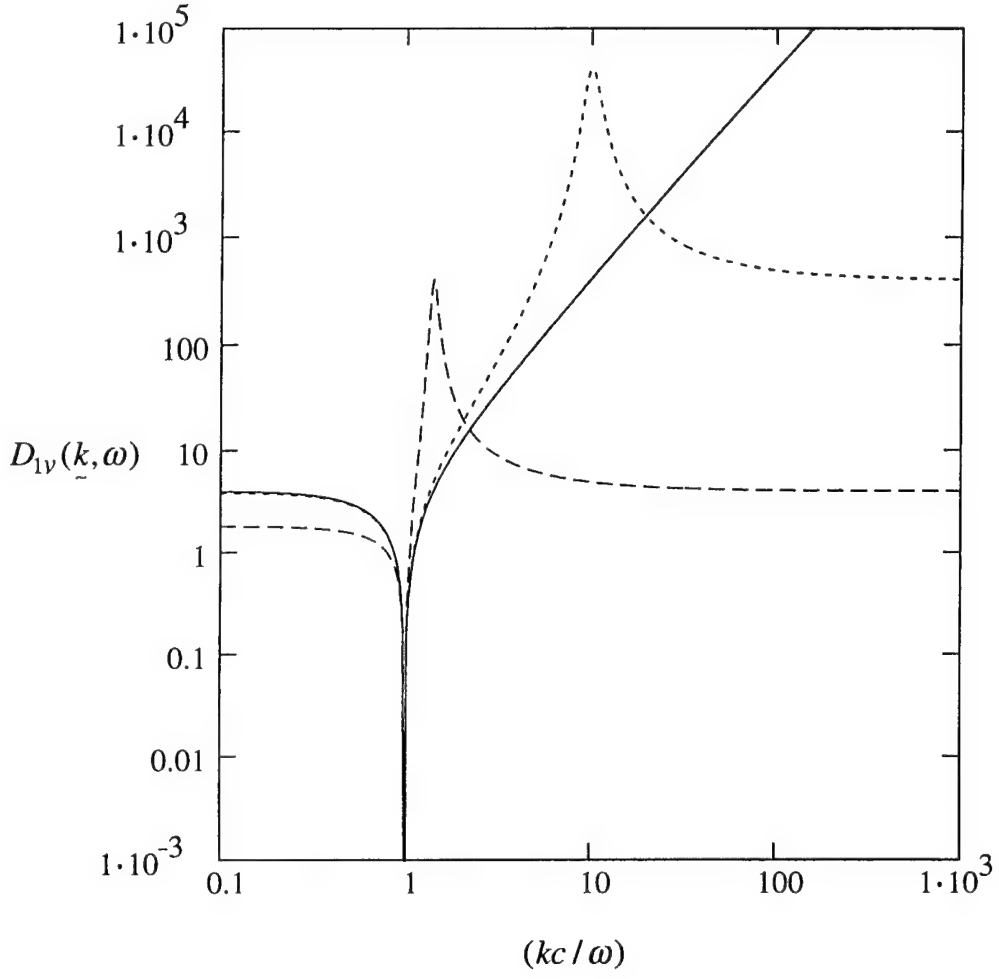

Fig. 8. The filtering efficiency $D_{1v}(\underset{\sim}{k},\omega) = \{[C_v(\underset{\sim}{k},\omega)\ E_p^v(\underset{\sim}{k},\omega)]\}$ of a compliantly conditioned boundary taking account of the conversion filtering efficiency, as a function of (kc/ω).

—— An ideal pressure release condition [β_o <<< 1].

····· Parametric values specified in Eq. (37a).

– – – Parametric values specified in Eq. (37b).

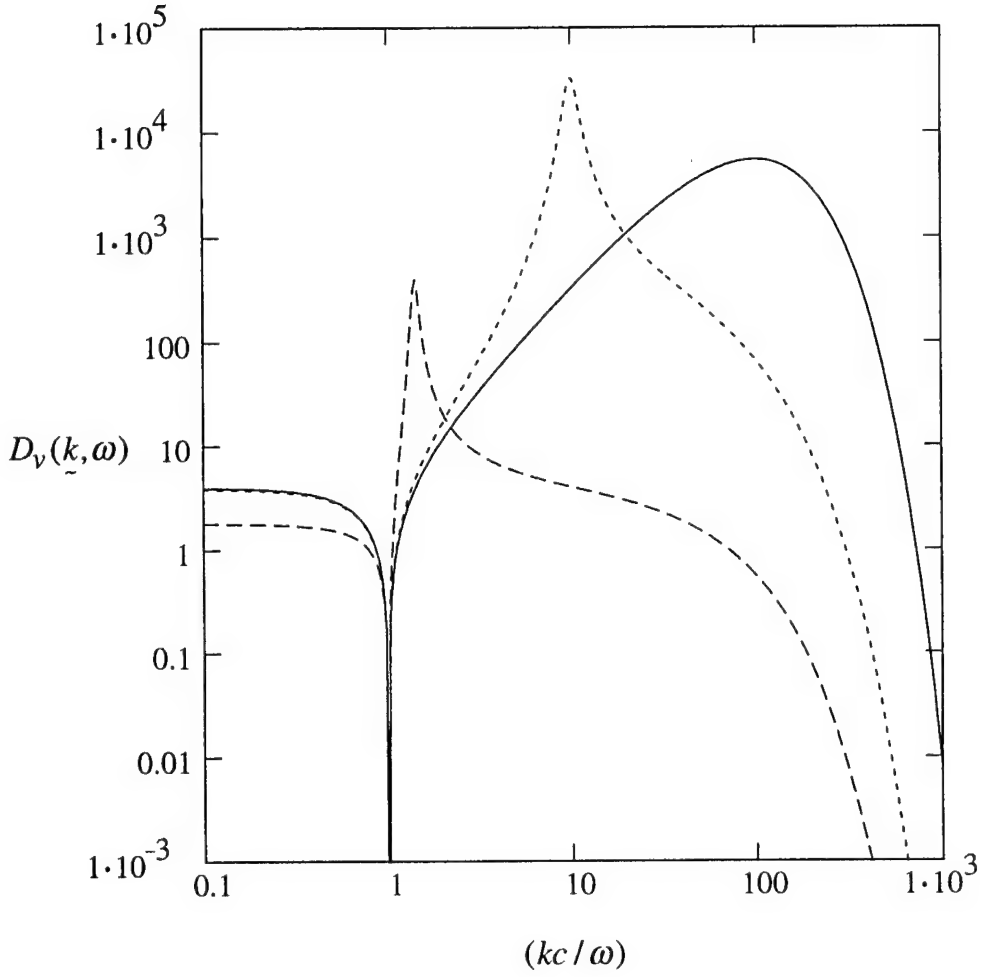

Fig. 9. The passive filtering efficiency $D_v(\underset{\sim}{k},\omega) = \{[C_v(\underset{\sim}{k},\omega)\ E_p^v(\underset{\sim}{k},\omega)\ B(\underset{\sim}{k},\omega)]\}$ of a blanketed compliantly conditioned boundary taking account of the conversion filtering efficiency, as a function of (kc/ω).

—— An ideal pressure release condition [β_o <<< 1].

····· Parametric values specified in Eq. (37a).

– – – Parametric values specified in Eq. (37b).

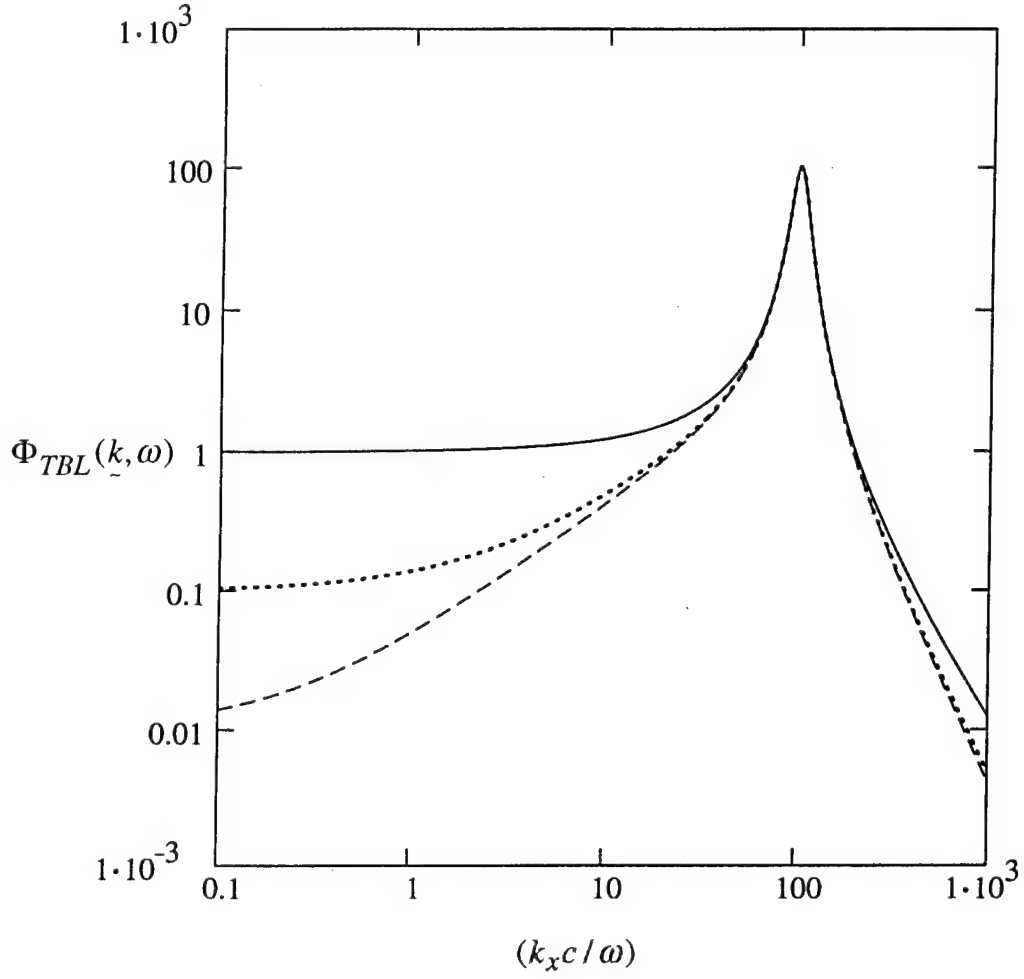

Fig. 10a. The spectral density $\Phi_{TBL}(\underset{\sim}{k},\omega)$ of a turbulent boundary layer (TBL) as a function of $(k_x c/\omega)$, with $(k_y c/\omega) \equiv 0$, $\alpha = 0.1$, $\beta = 3\alpha$, —— $a = 1$, ····· $a = 0.1$ and – – – $a = 0.01$. [cf. Eqs. (49) and (50)].

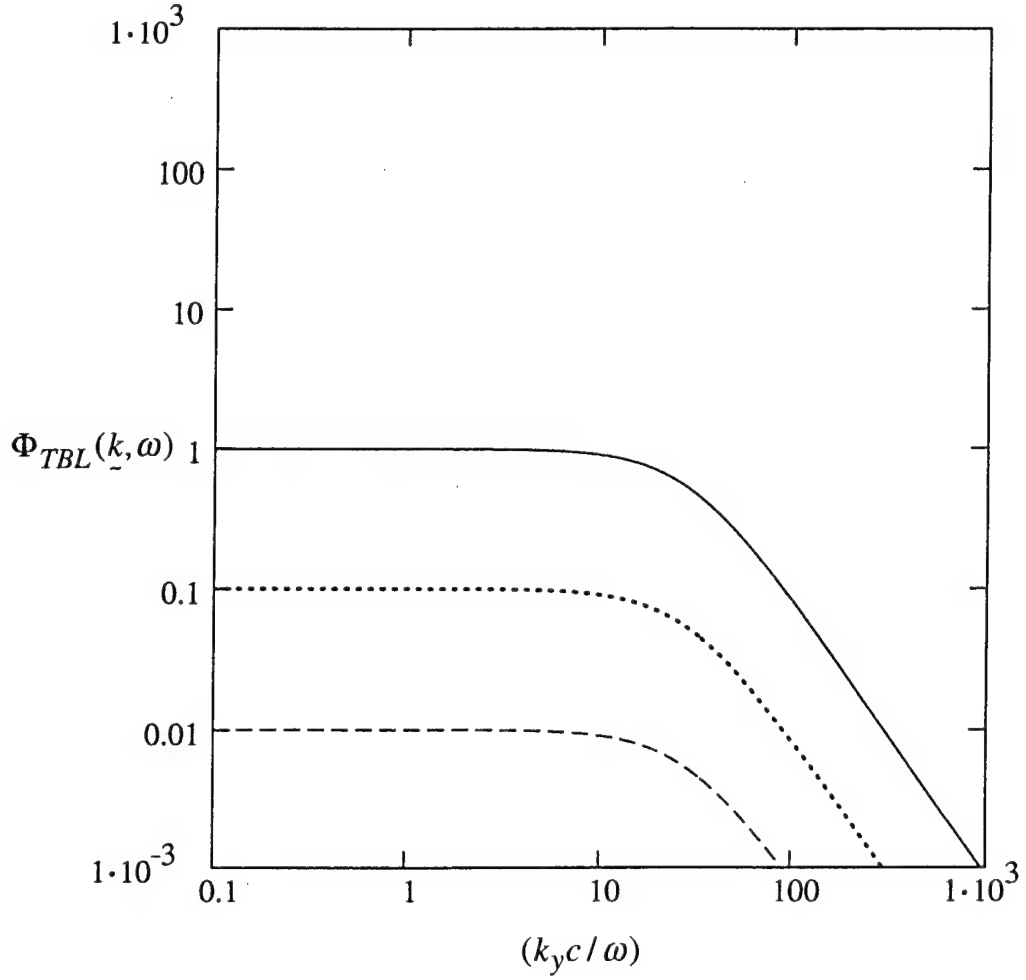

Fig. 10b. The spectral density $\Phi_{TBL}(\underset{\sim}{k},\omega)$ of a turbulent boundary layer (TBL), as a function of $(k_y c/\omega)$, with $(k_x c/\omega) \equiv 0$, $\alpha = 0.1$, $\beta = 3\alpha$, —— $a = 1$, ····· $a = 0.1$ and – – – $a = 0.01$. [cf. Eqs. (49) and (50)].

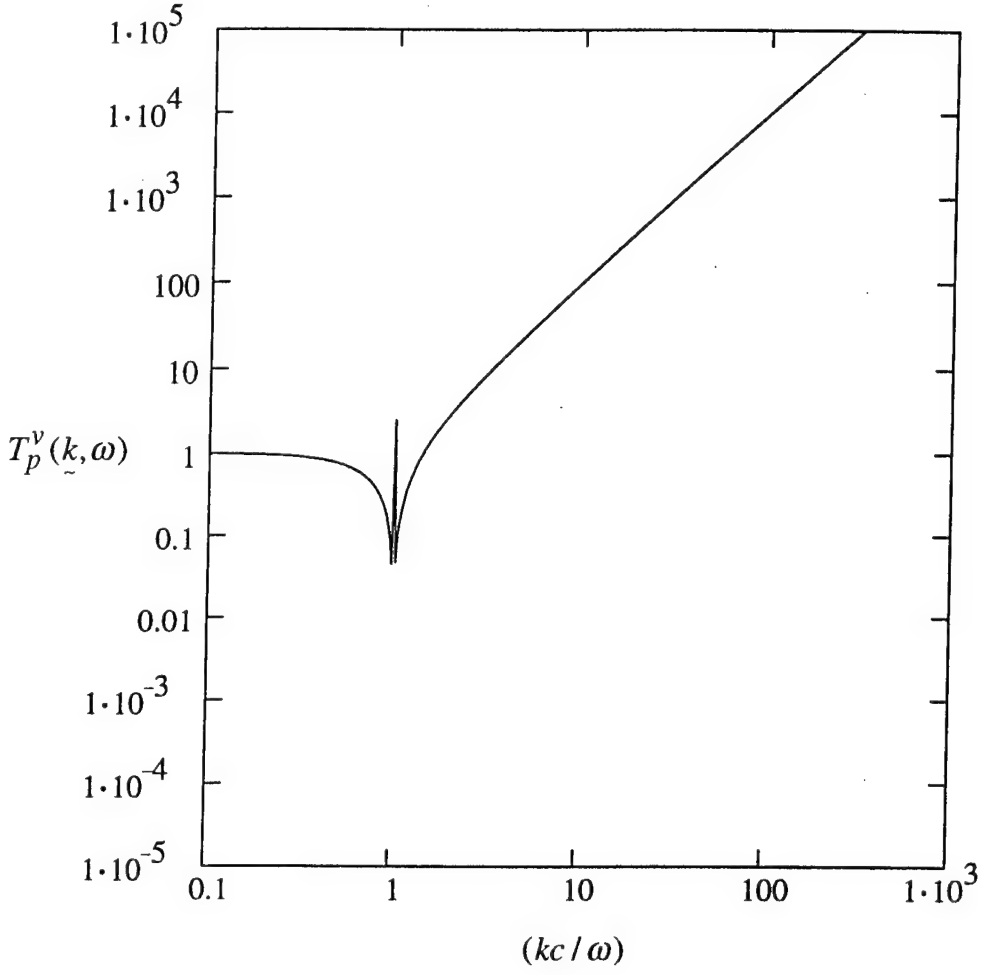

Fig. 11a. The factor $T_p^v(\underset{\sim}{k},\omega) = [D_{1v}(\underset{\sim}{k},\omega)/C_p(\underset{\sim}{k},\omega)]$, as a function of (kc/ω).

[cf. Eqs. (44) and (45).]

Ideal conditions on both the pressure and velocity arrays [(β) and $(\zeta) <<< 1$] and [$\beta_o <<< 1$].

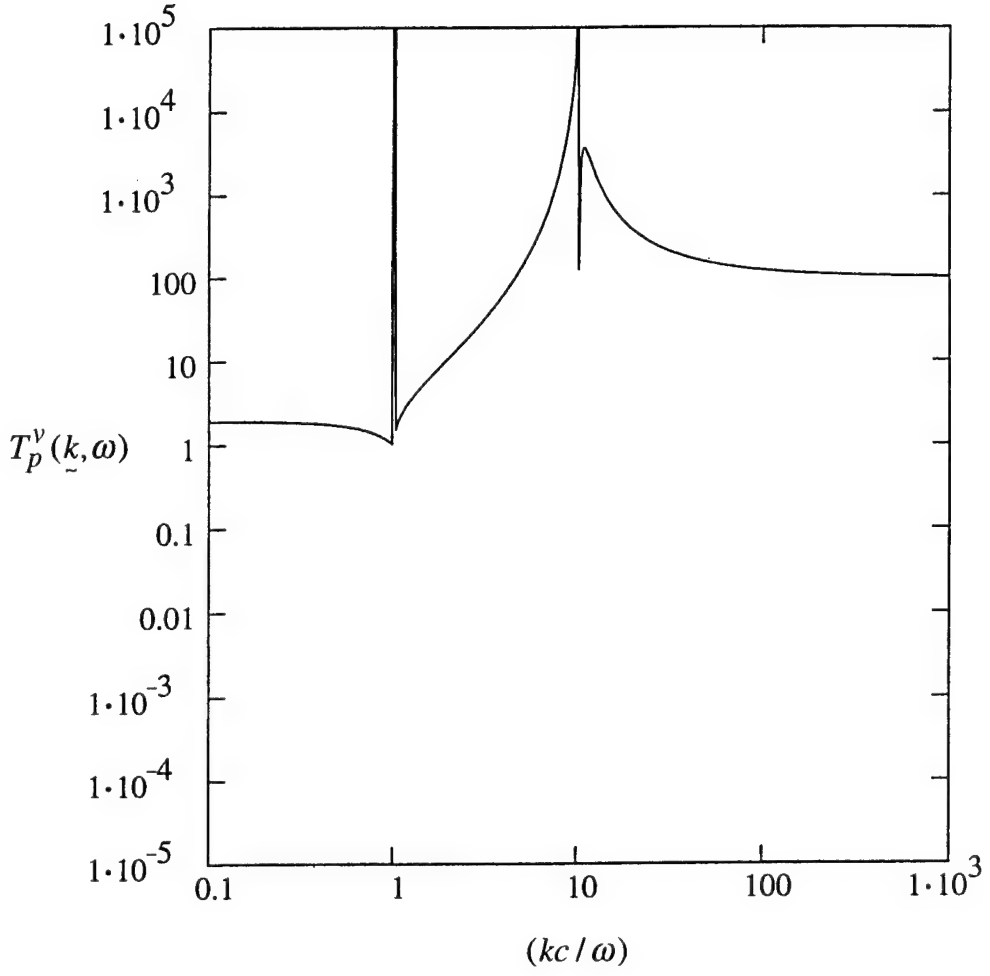

Fig. 11b. The factor $T_p^{\nu}(\underset{\sim}{k},\omega) = [D_{1\nu}(\underset{\sim}{k},\omega)/C_p(\underset{\sim}{k},\omega)]$, as a function of (kc/ω).

[cf. Eqs. (44) and (45).]

Parametric values specified in Eqs. (21a) and (37a).

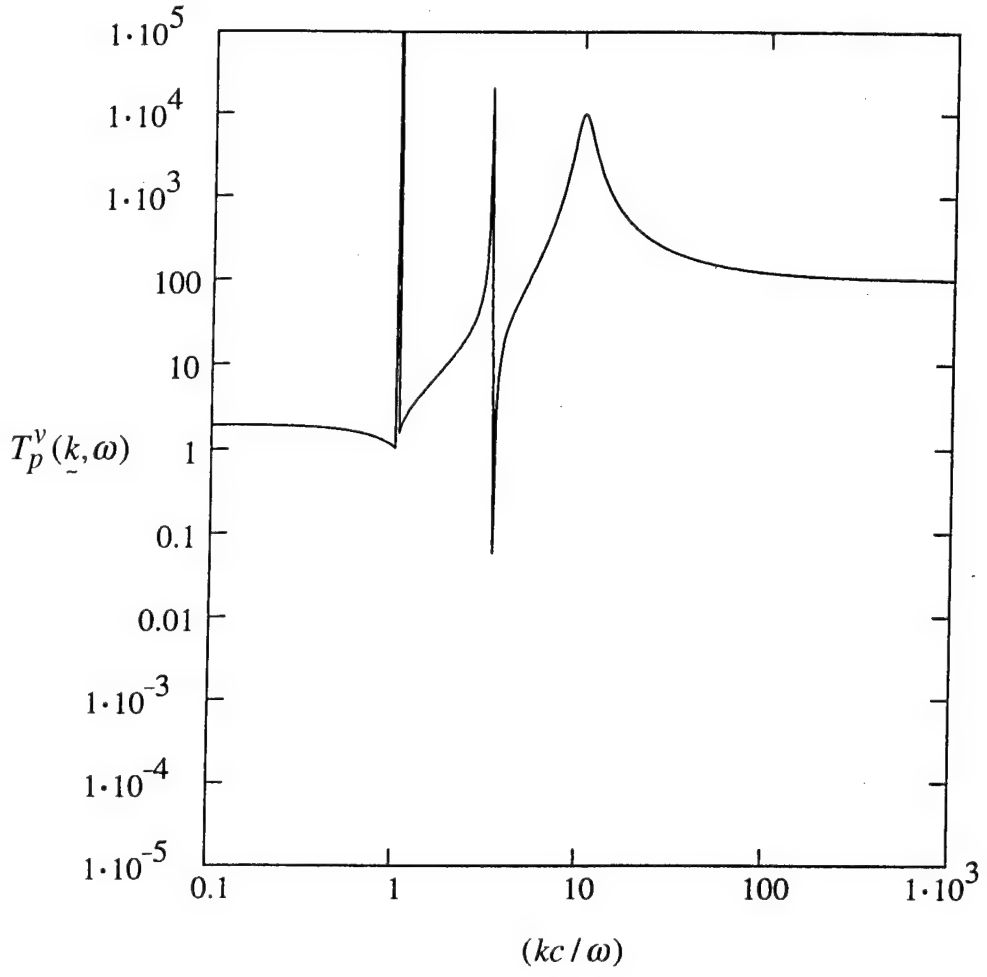

Fig. 11c. The factor $T_p^v(\underset{\sim}{k},\omega) = [D_{1v}(\underset{\sim}{k},\omega)/C_p(\underset{\sim}{k},\omega)]$, as a function of (kc/ω).

[cf. Eqs. (44) and (45).]

Parametric values specified in Eqs. (21b) and (37a).

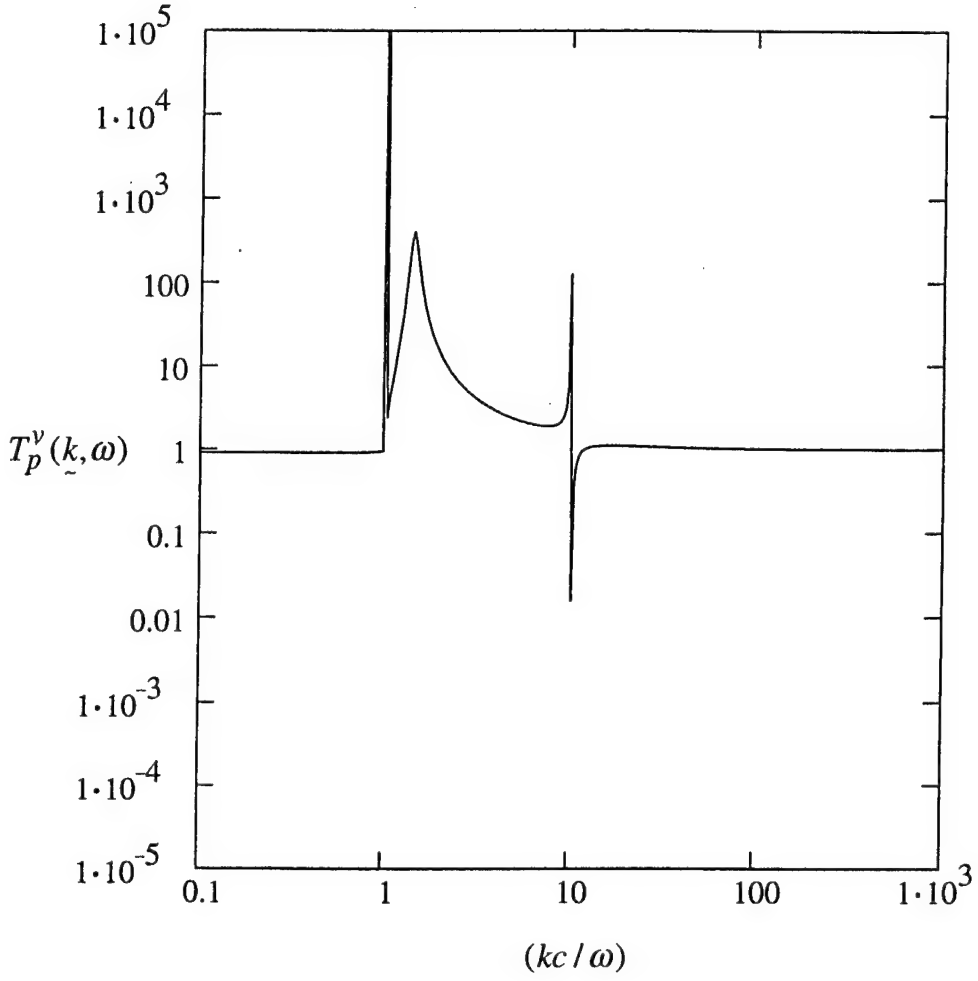

Fig. 11d. The factor $T_p^{\nu}(\underset{\sim}{k},\omega) = [D_{1\nu}(\underset{\sim}{k},\omega)/C_p(\underset{\sim}{k},\omega)]$, as a function of (kc/ω).

[cf. Eqs. (44) and (45).]

Parametric values specified in Eqs. (21a) and (37b).

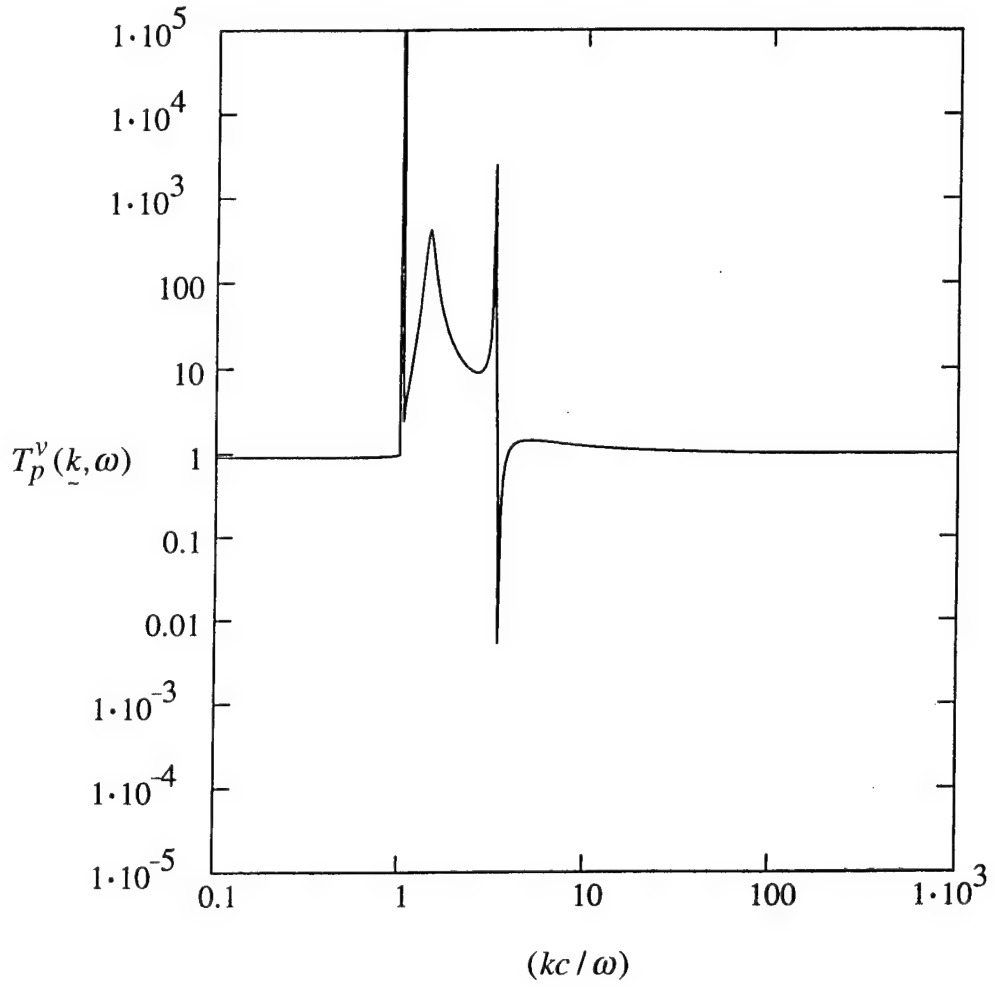

Fig. 11e. The factor $T_p^{\nu}(\underset{\sim}{k},\omega) = [D_{1\nu}(\underset{\sim}{k},\omega)/C_p(\underset{\sim}{k},\omega)]$, as a function of (kc/ω).

[cf. Eqs. (44) and (45).]

Parametric values specified in Eqs. (21b) and (37b).

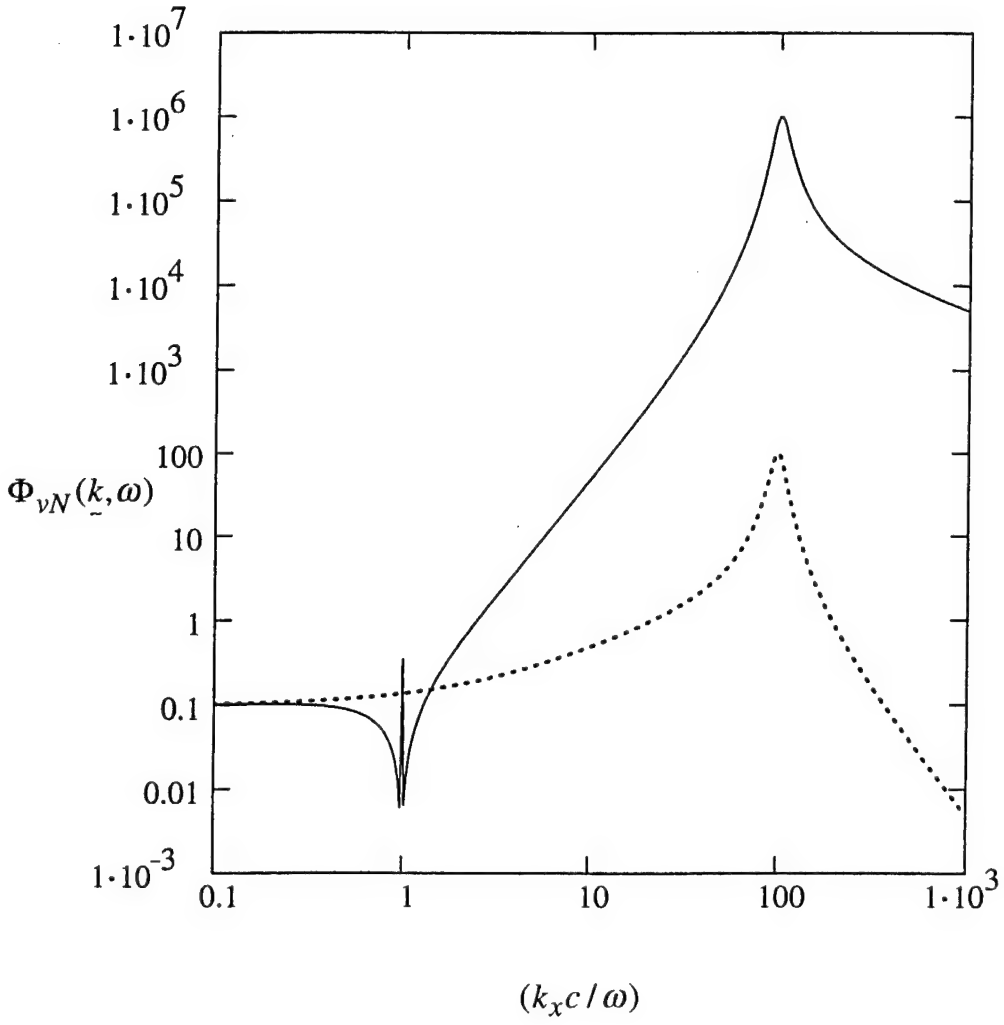

Fig. 12a. The equivalent spectral density $\Phi_{vN}(\underset{\sim}{k},\omega)$ of the pressure in a turbulent boundary layer (TBL), as a function of $(k_y c/\omega)$ with $(k_x c/\omega) \equiv 0$, —— $\Phi_{vN}(\underset{\sim}{k},\omega)$ and superimposed, for comparison, ····· $\Phi_{pN}(\underset{\sim}{k},\omega)$. As in 11a.

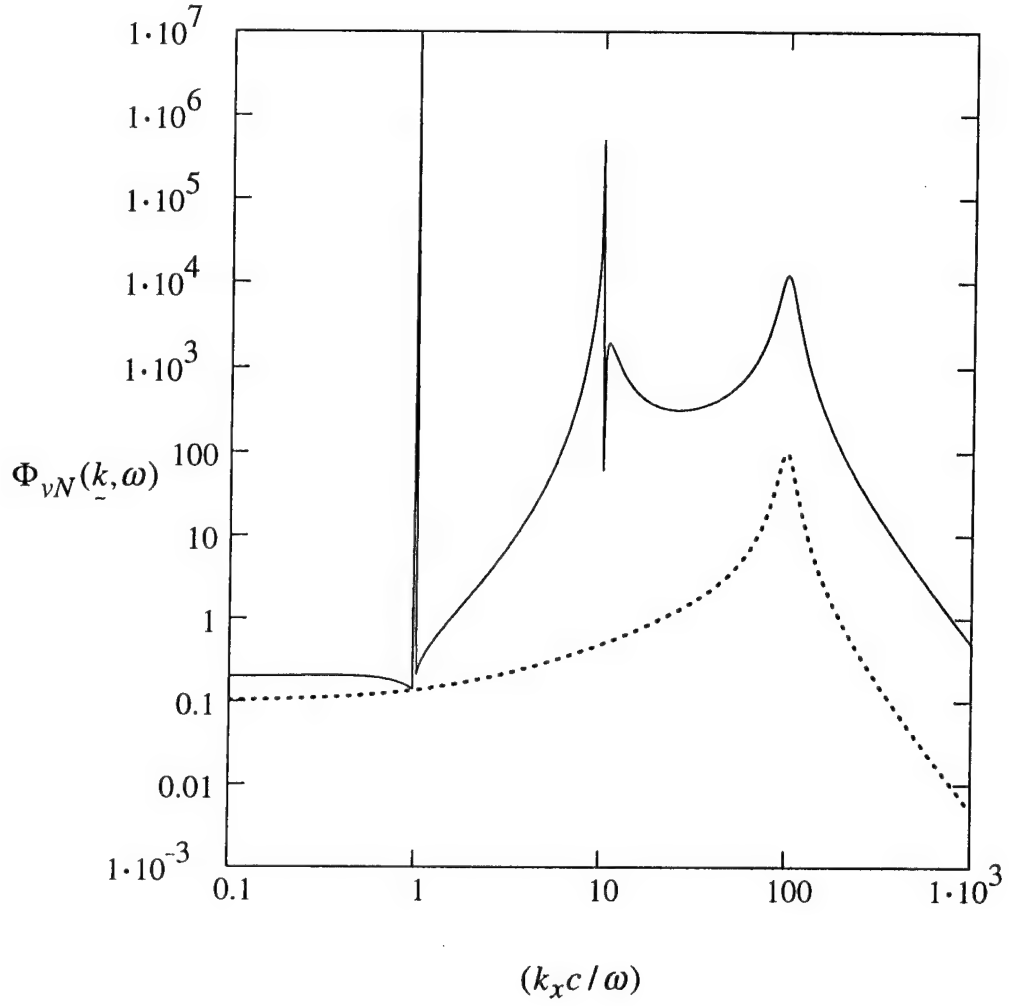

Fig. 12b. The equivalent spectral density $\Phi_{vN}(\underset{\sim}{k},\omega)$ of the pressure in a turbulent boundary layer (TBL), as a function of $(k_x c/\omega)$ with $(k_y c/\omega) \equiv 0$, —— $\Phi_{vN}(\underset{\sim}{k},\omega)$ and superimposed, for comparison, ····· $\Phi_{pN}(\underset{\sim}{k},\omega)$. As in 11b.

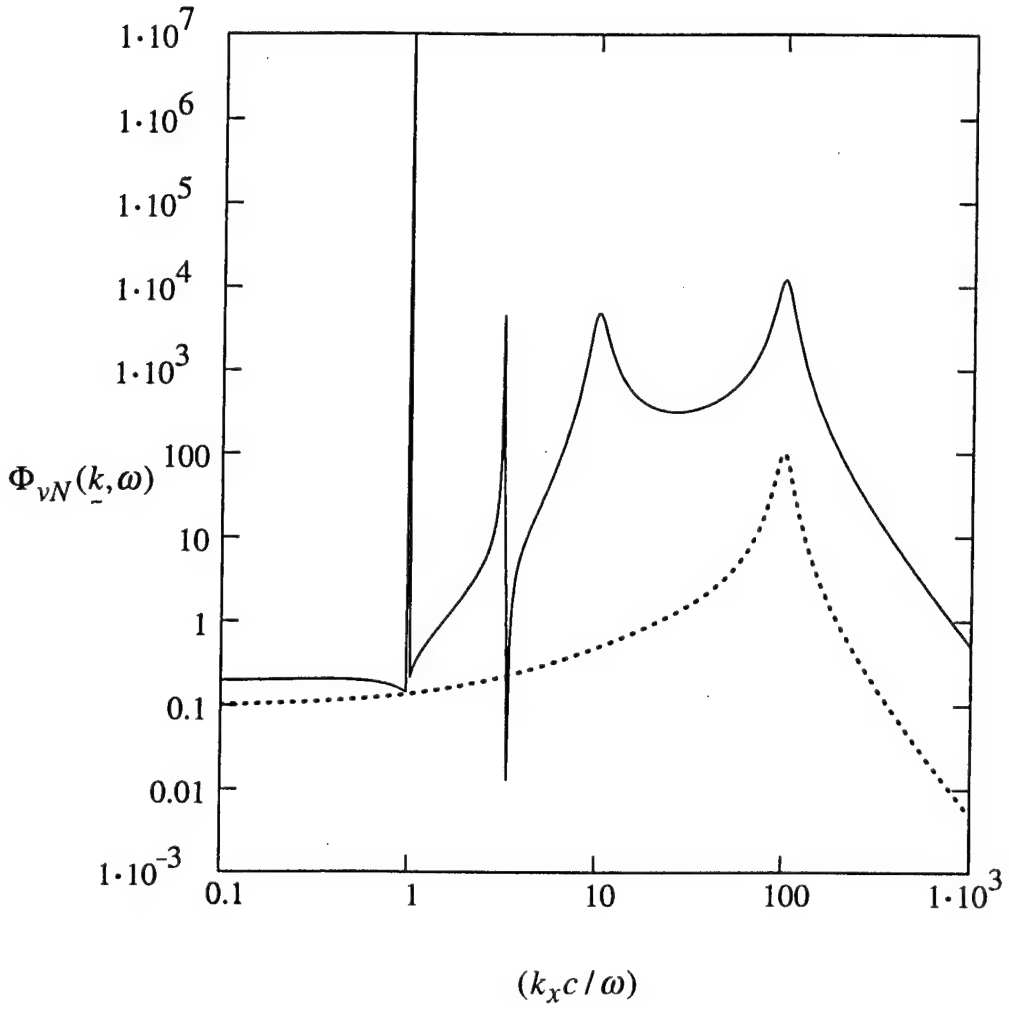

Fig. 12c. The equivalent spectral density $\Phi_{vN}(\underset{\sim}{k},\omega)$ of the pressure in a turbulent boundary layer (TBL), as a function of $(k_x c/\omega)$ with $(k_y c/\omega) \equiv 0$, —— $\Phi_{vN}(\underset{\sim}{k},\omega)$ and superimposed, for comparison, ····· $\Phi_{pN}(\underset{\sim}{k},\omega)$. As in 11c.

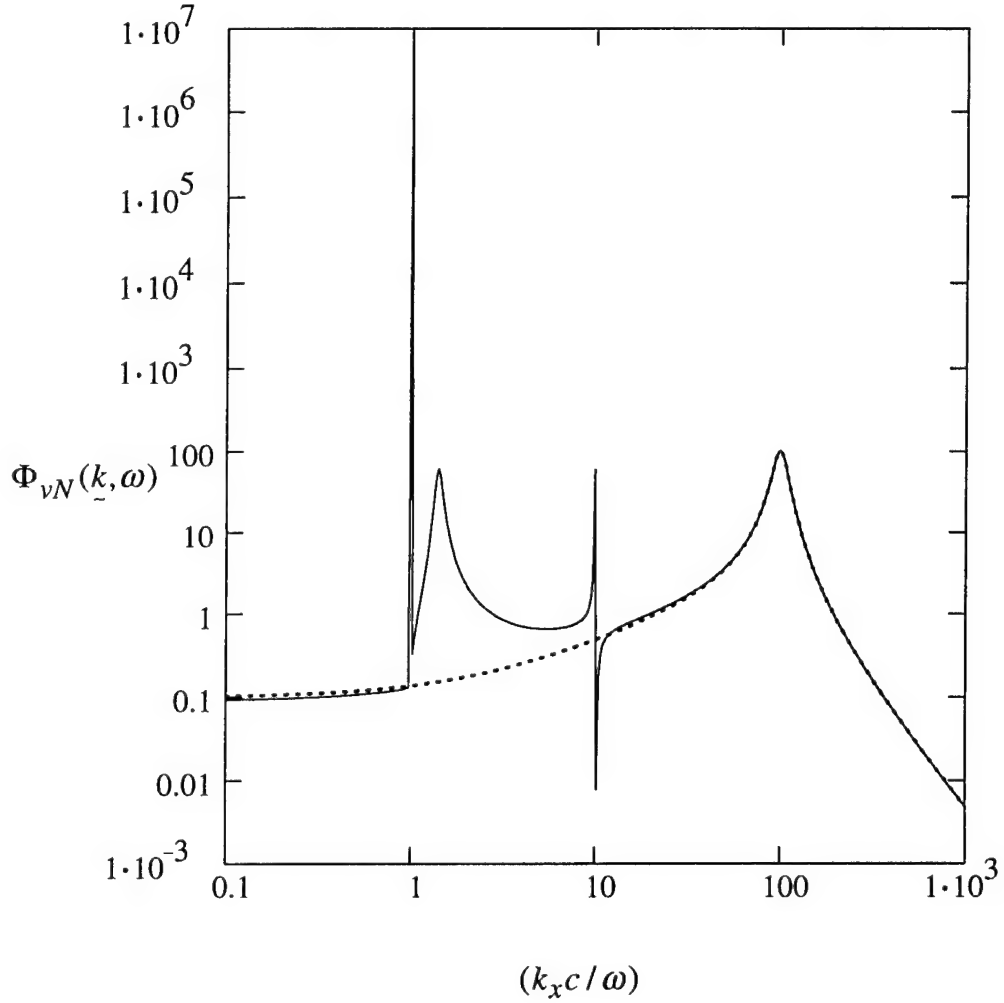

Fig. 12d. The equivalent spectral density $\Phi_{vN}(\underset{\sim}{k},\omega)$ of the pressure in a turbulent boundary layer (TBL), as a function of $(k_x c/\omega)$ with $(k_y c/\omega) \equiv 0$, —— $\Phi_{vN}(\underset{\sim}{k},\omega)$ and superimposed, for comparison, ····· $\Phi_{pN}(\underset{\sim}{k},\omega)$. As in 11d.

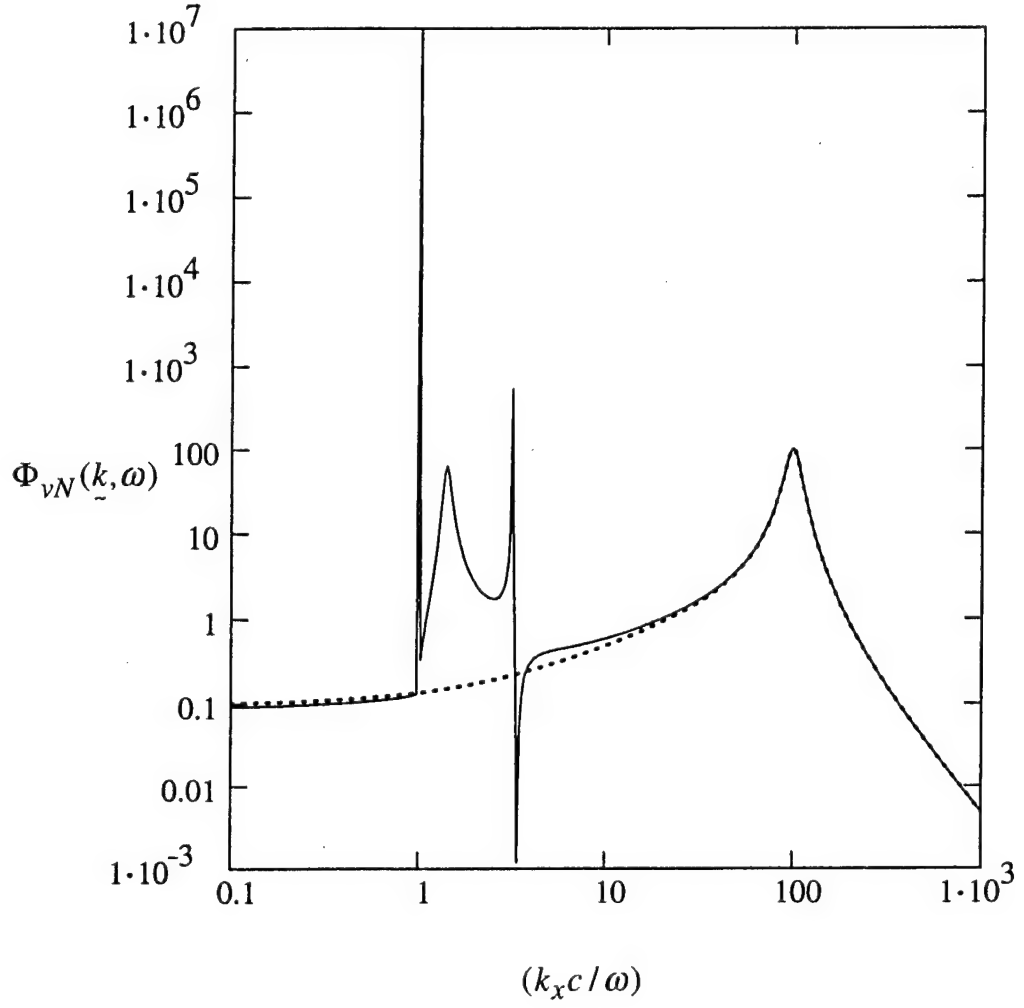

Fig. 12e. The equivalent spectral density $\Phi_{vN}(\underset{\sim}{k},\omega)$ of the pressure in a turbulent boundary layer (TBL), as a function of $(k_x c/\omega)$ with $(k_y c/\omega) \equiv 0$, —— $\Phi_{vN}(\underset{\sim}{k},\omega)$ and superimposed, for comparison, ····· $\Phi_{pN}(\underset{\sim}{k},\omega)$. As in 11e.

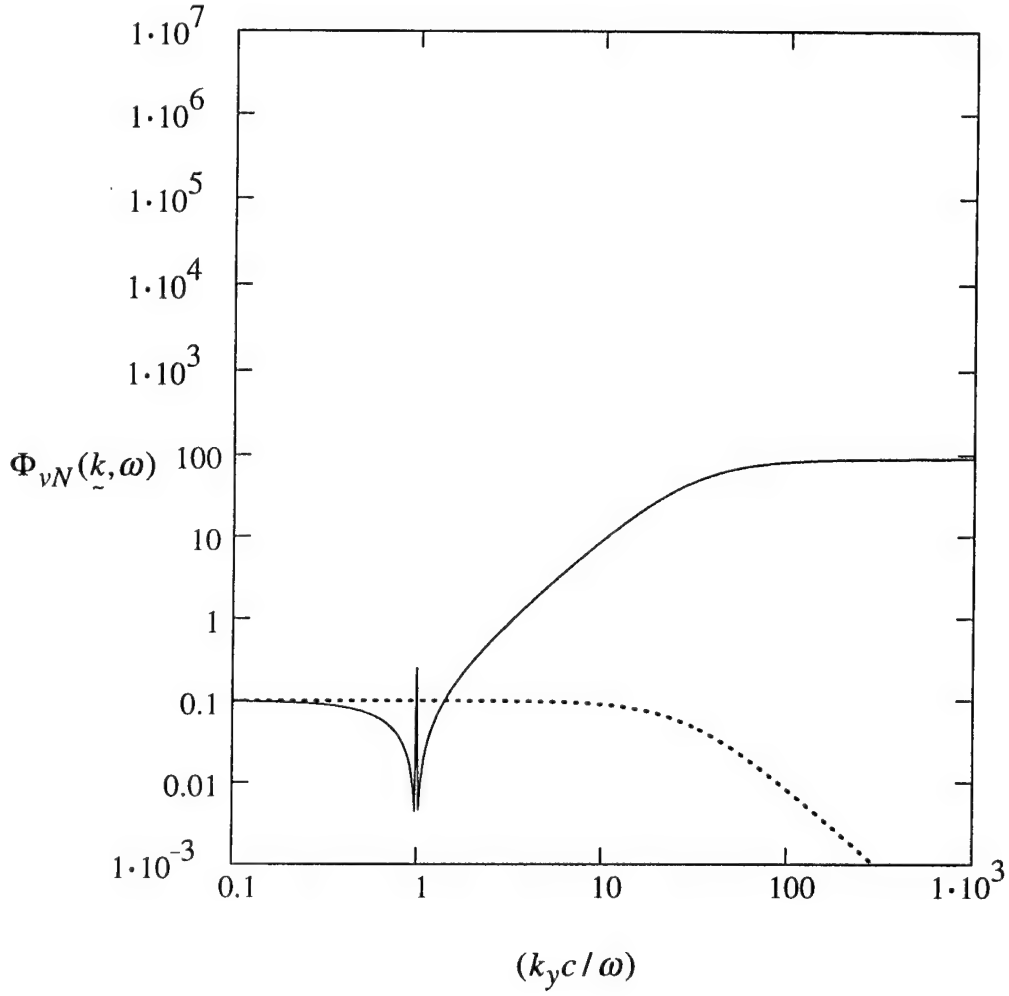

Fig. 12.1a. The equivalent spectral density $\Phi_{vN}(\underset{\sim}{k},\omega)$ of the pressure in a turbulent boundary layer (TBL), as a function of $(k_y c/\omega)$ with $(k_x c/\omega) \equiv 0$, —— $\Phi_{vN}(\underset{\sim}{k},\omega)$ and superimposed, for comparison, ····· $\Phi_{pN}(\underset{\sim}{k},\omega)$. As in 11a.

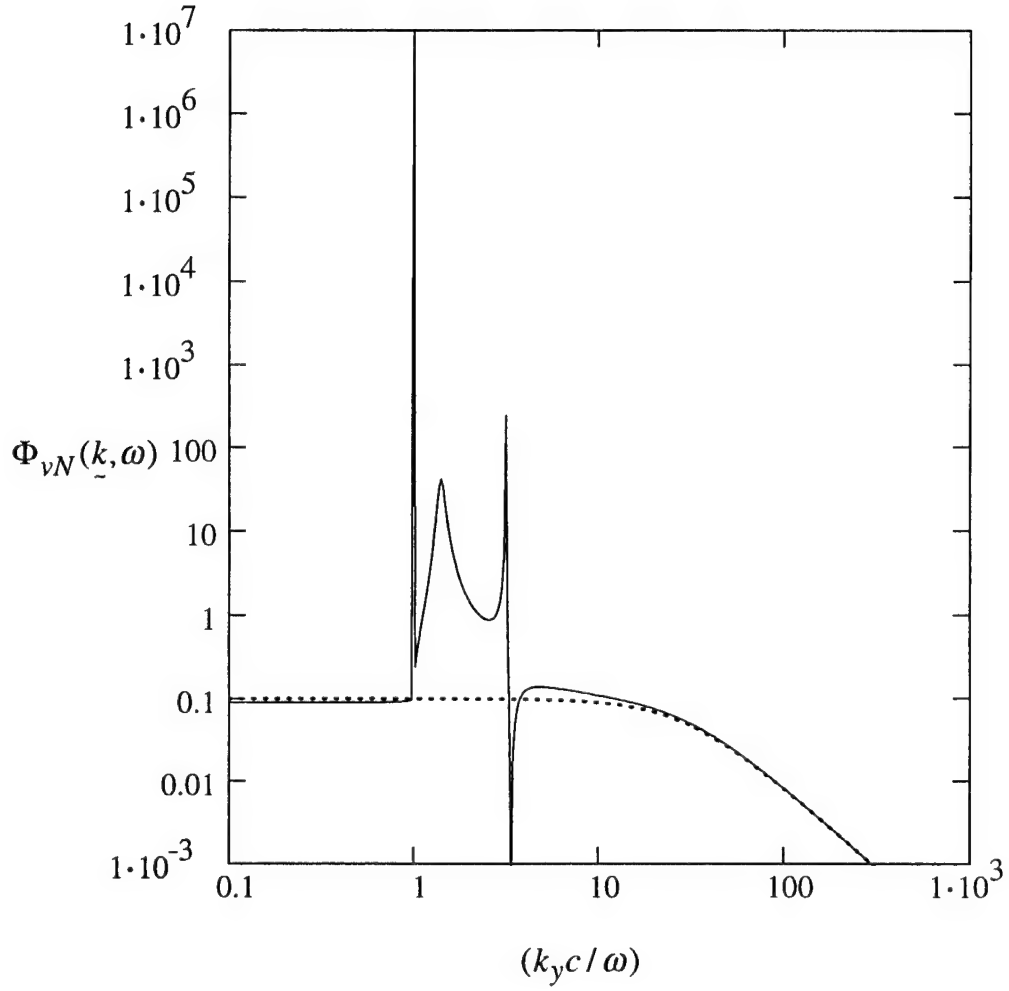

Fig. 12.1c. The equivalent spectral density $\Phi_{vN}(\underset{\sim}{k},\omega)$ of the pressure in a turbulent boundary layer (TBL), as a function of $(k_y c/\omega)$ with $(k_x c/\omega) \equiv 0$, —— $\Phi_{vN}(\underset{\sim}{k},\omega)$ and superimposed, for comparison, ····· $\Phi_{pN}(\underset{\sim}{k},\omega)$. As in 11c.

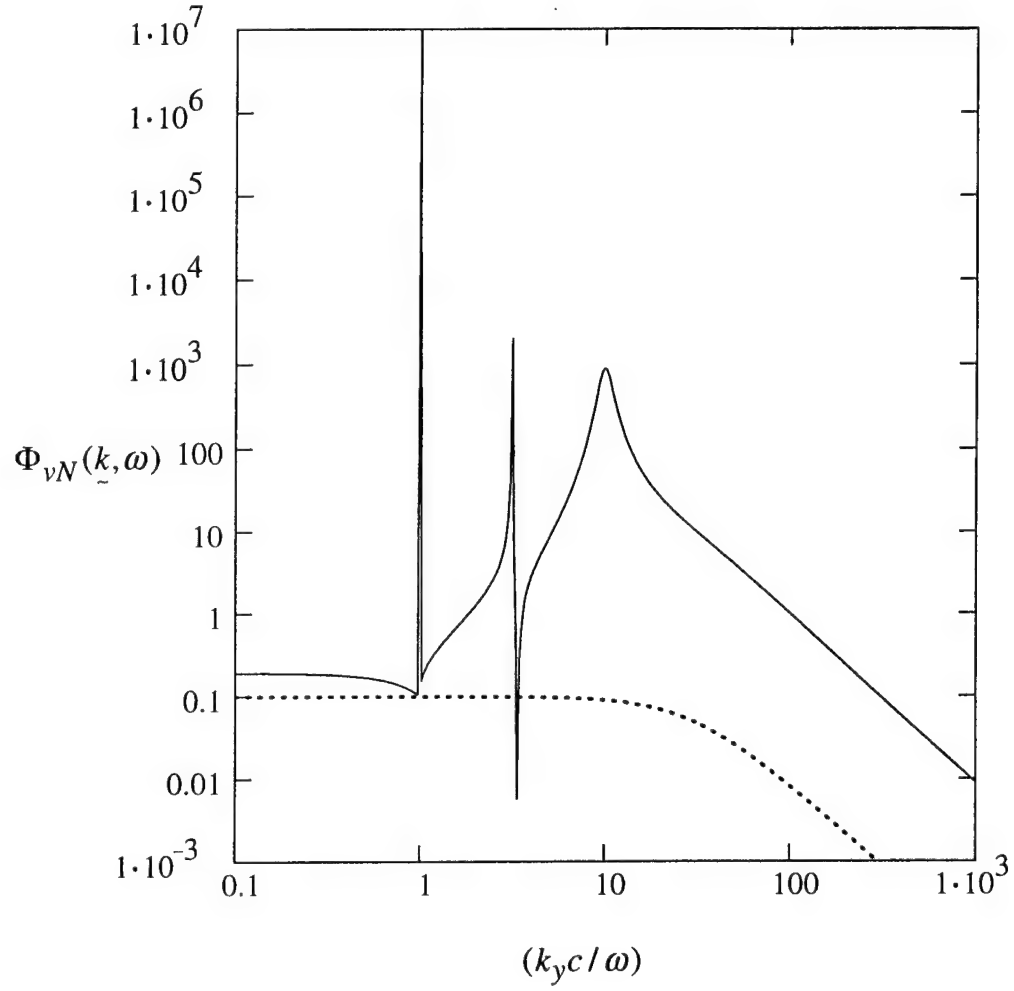

Fig. 12.1e. The equivalent spectral density $\Phi_{vN}(\underset{\sim}{k},\omega)$ of the pressure in a turbulent boundary layer (TBL), as a function of $(k_y c/\omega)$ with $(k_x c/\omega) \equiv 0$, —— $\Phi_{vN}(\underset{\sim}{k},\omega)$ and superimposed, for comparison, ····· $\Phi_{pN}(\underset{\sim}{k},\omega)$. As in 11c.

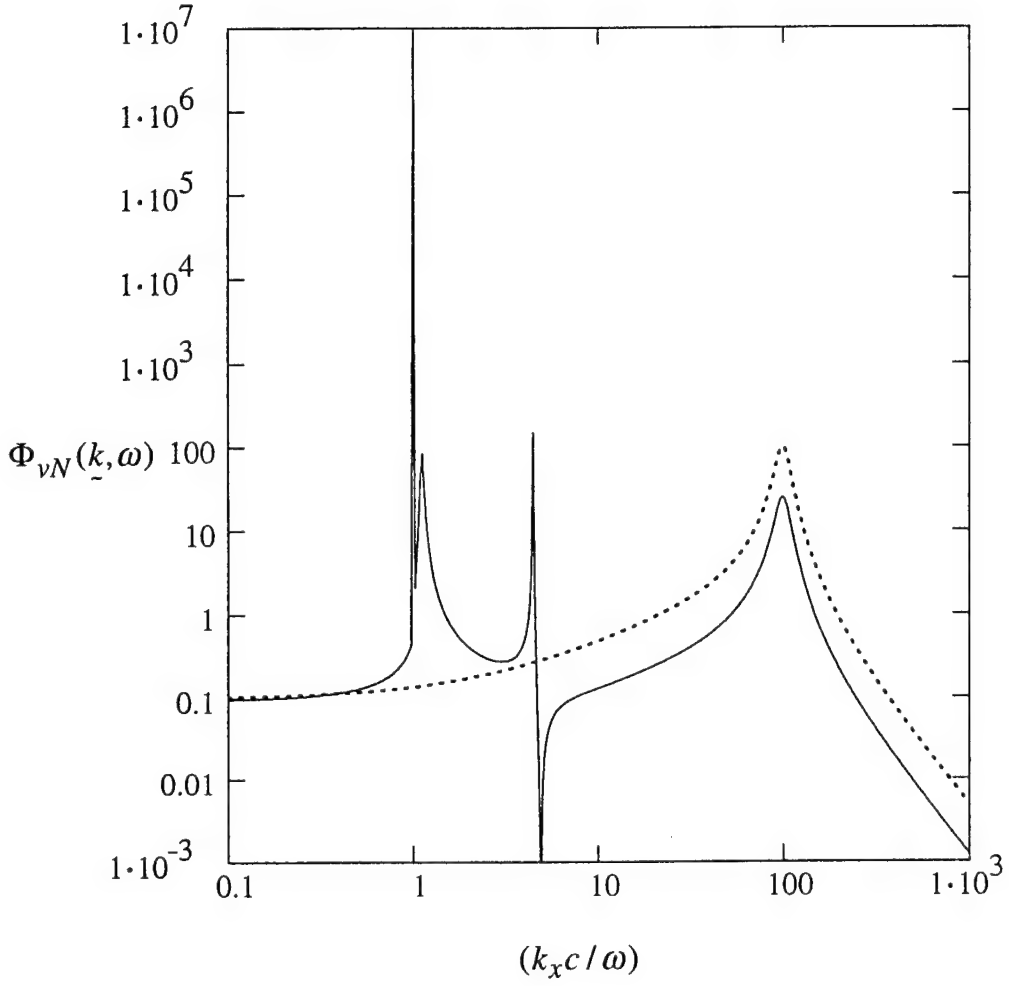

Fig. 13a. The equivalent spectral density $\Phi_{vN}(\underset{\sim}{k},\omega)$ of the pressure in a turbulent boundary layer (TBL), as a function of $(k_x c/\omega)$ with $(k_y c/\omega) \equiv 0$. The parameters (ε_o) and (ε_c) are both set equal to 10^{-1}.
$(\omega_o/\omega) = (\omega_c/\omega) = 20$.

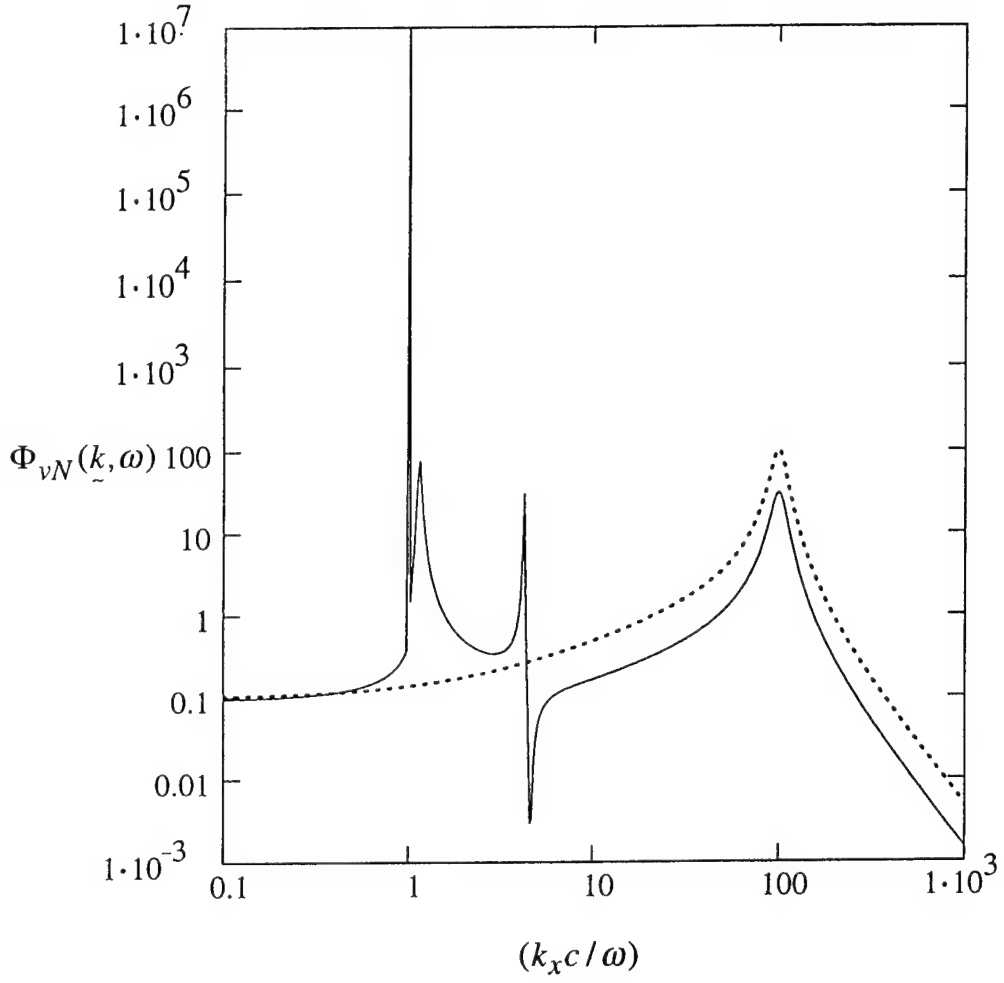

Fig. 13b. The equivalent spectral density $\Phi_{vN}(\underset{\sim}{k}, \omega)$ of the pressure in a turbulent boundary layer (TBL), as a function of $(k_x c / \omega)$ with $(k_y c / \omega) \equiv 0$. The parameters (ε_o) and (ε_c) are both set equal to 10^{-1}.
$(\omega_o / \omega) = (\omega_c / \omega) = 18$.

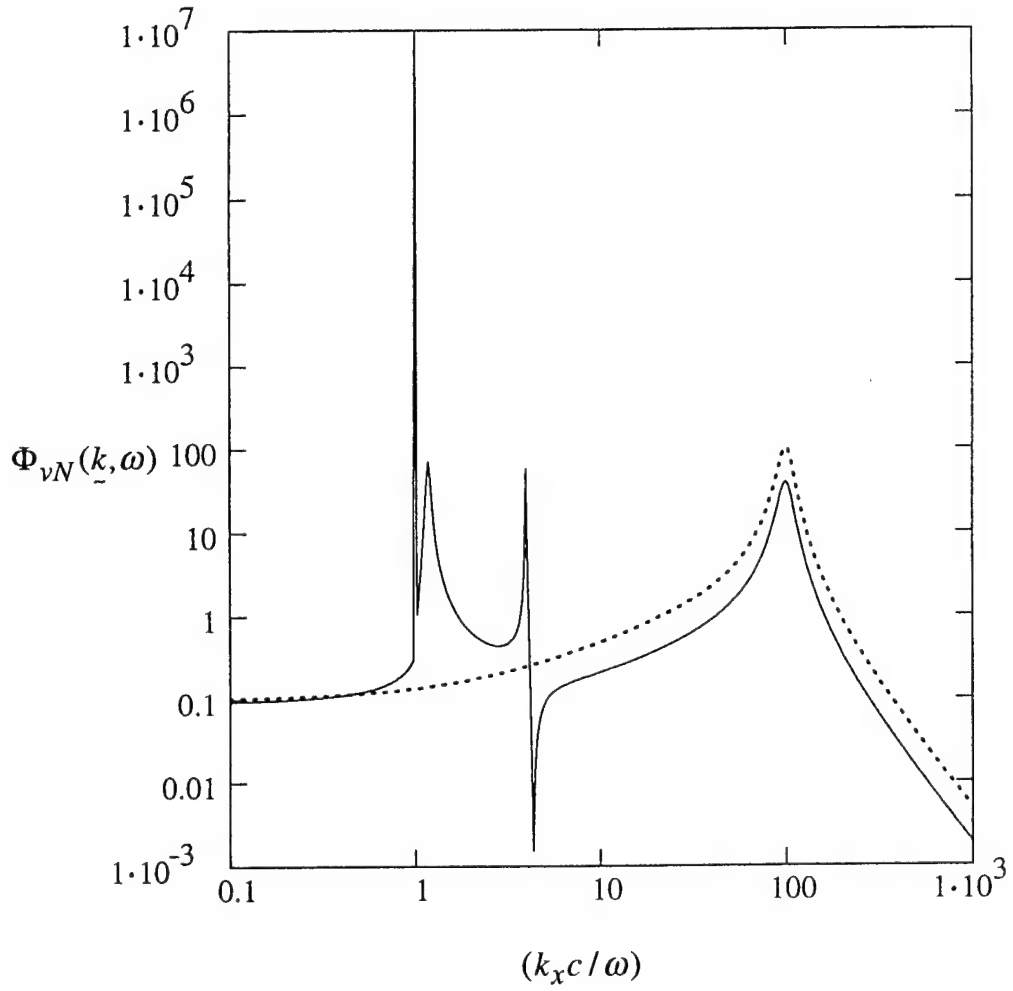

Fig. 13c. The equivalent spectral density $\Phi_{vN}(\underset{\sim}{k},\omega)$ of the pressure in a turbulent boundary layer (TBL), as a function of $(k_x c/\omega)$ with $(k_y c/\omega) \equiv 0$. The parameters (ε_o) and (ε_c) are both set equal to 10^{-1}.
$(\omega_o/\omega) = (\omega_c/\omega) = 16$.

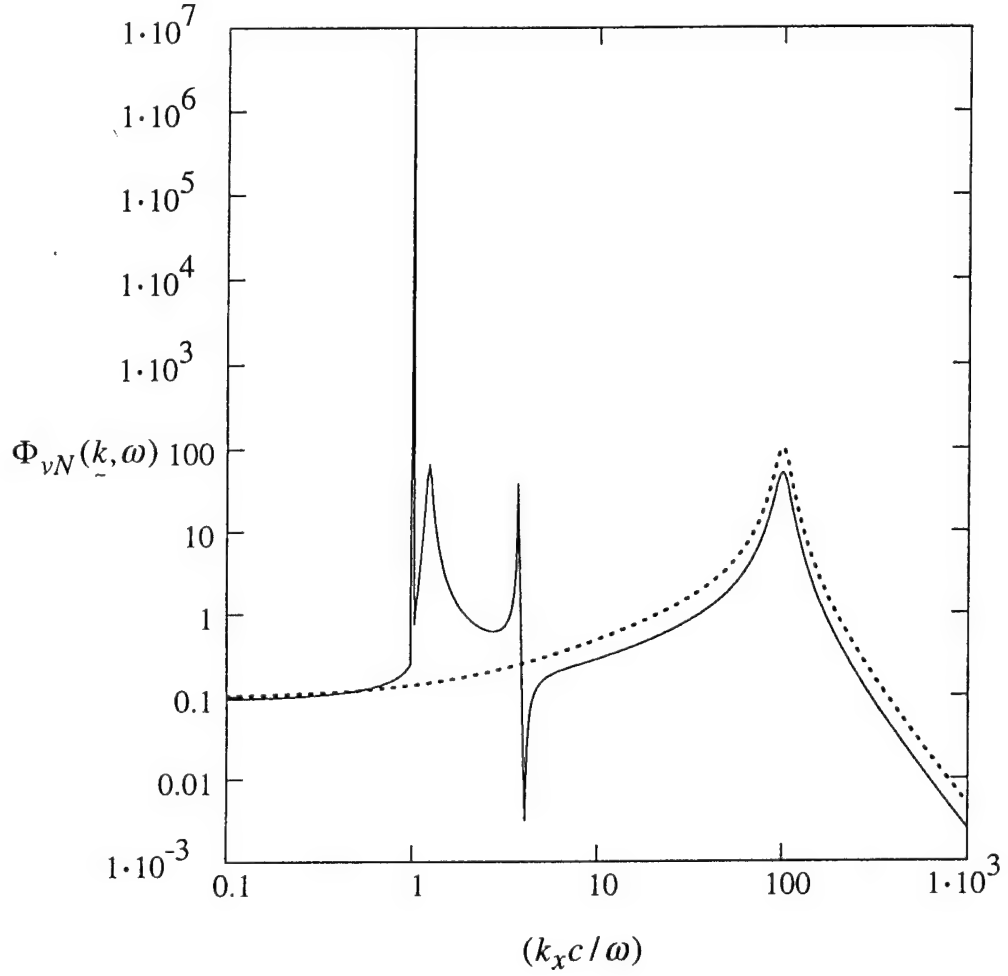

Fig. 13d. The equivalent spectral density $\Phi_{vN}(\underset{\sim}{k},\omega)$ of the pressure in a turbulent boundary layer (TBL), as a function of $(k_x c/\omega)$ with $(k_y c/\omega) \equiv 0$. The parameters (ε_o) and (ε_c) are both set equal to 10^{-1}.
$(\omega_o/\omega) = (\omega_c/\omega) = 14$.

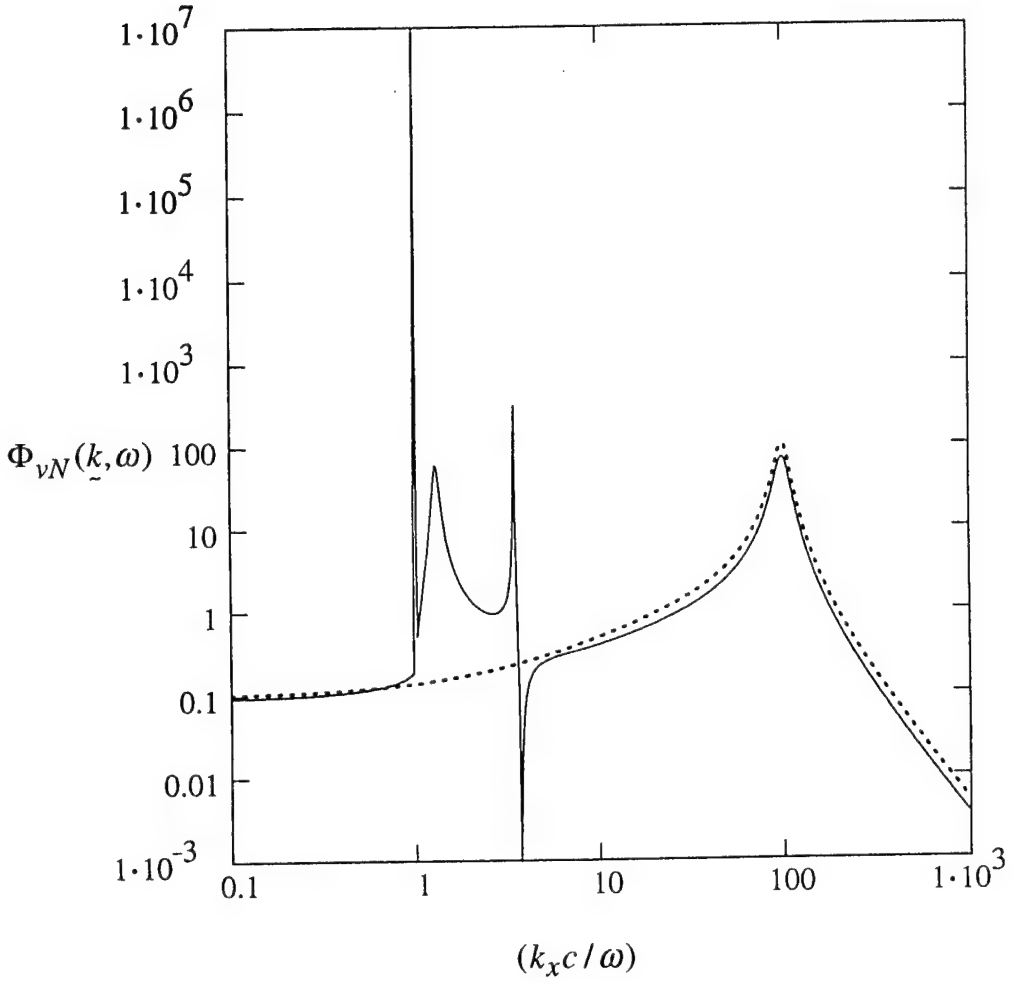

Fig. 13e. The equivalent spectral density $\Phi_{vN}(\underset{\sim}{k},\omega)$ of the pressure in a turbulent boundary layer (TBL), as a function of $(k_x c/\omega)$ with $(k_y c/\omega) \equiv 0$. The parameters (ε_o) and (ε_c) are both set equal to 10^{-1}.
$(\omega_o/\omega) = (\omega_c/\omega) = 12$.

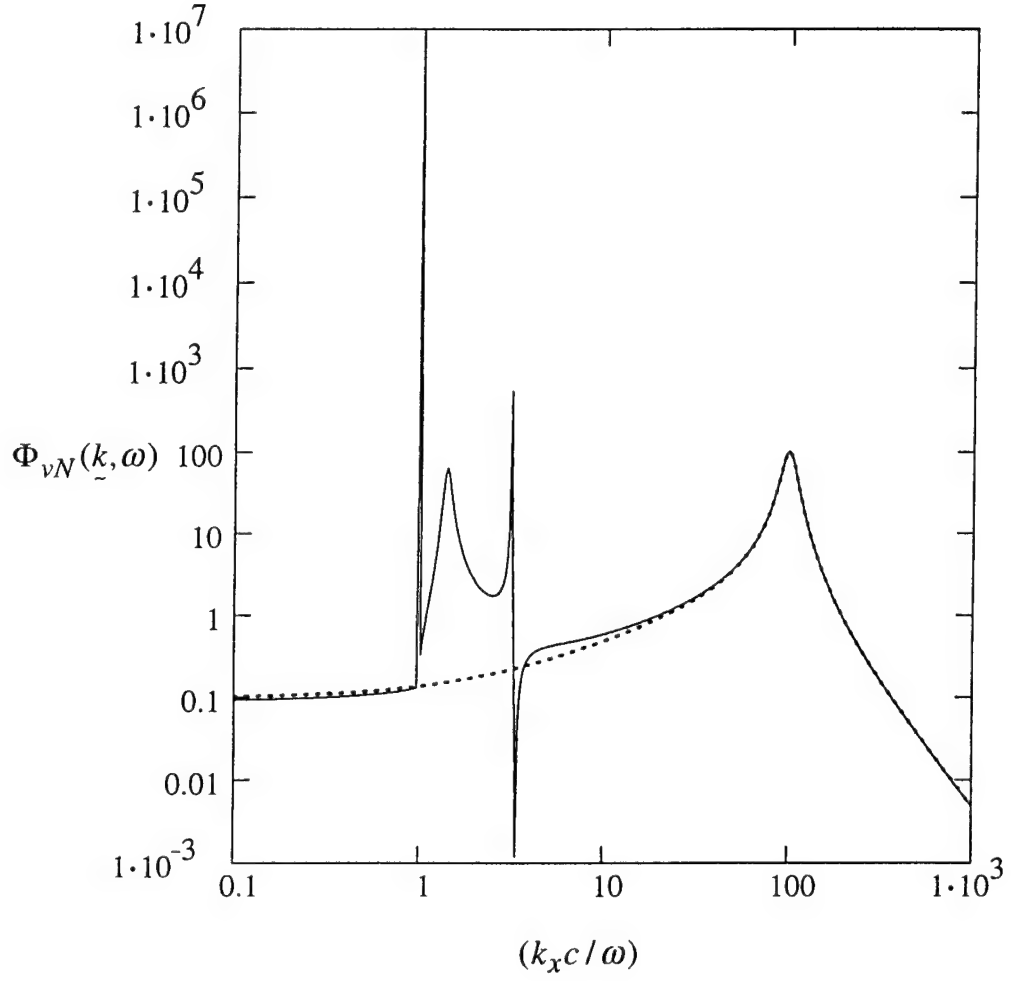

Fig. 13f. The equivalent spectral density $\Phi_{vN}(\underset{\sim}{k},\omega)$ of the pressure in a turbulent boundary layer (TBL), as a function of $(k_x c/\omega)$ with $(k_y c/\omega) \equiv 0$. The parameters (ε_o) and (ε_c) are both set equal to 10^{-1}.
$(\omega_o/\omega) = (\omega_c/\omega) = 10$.

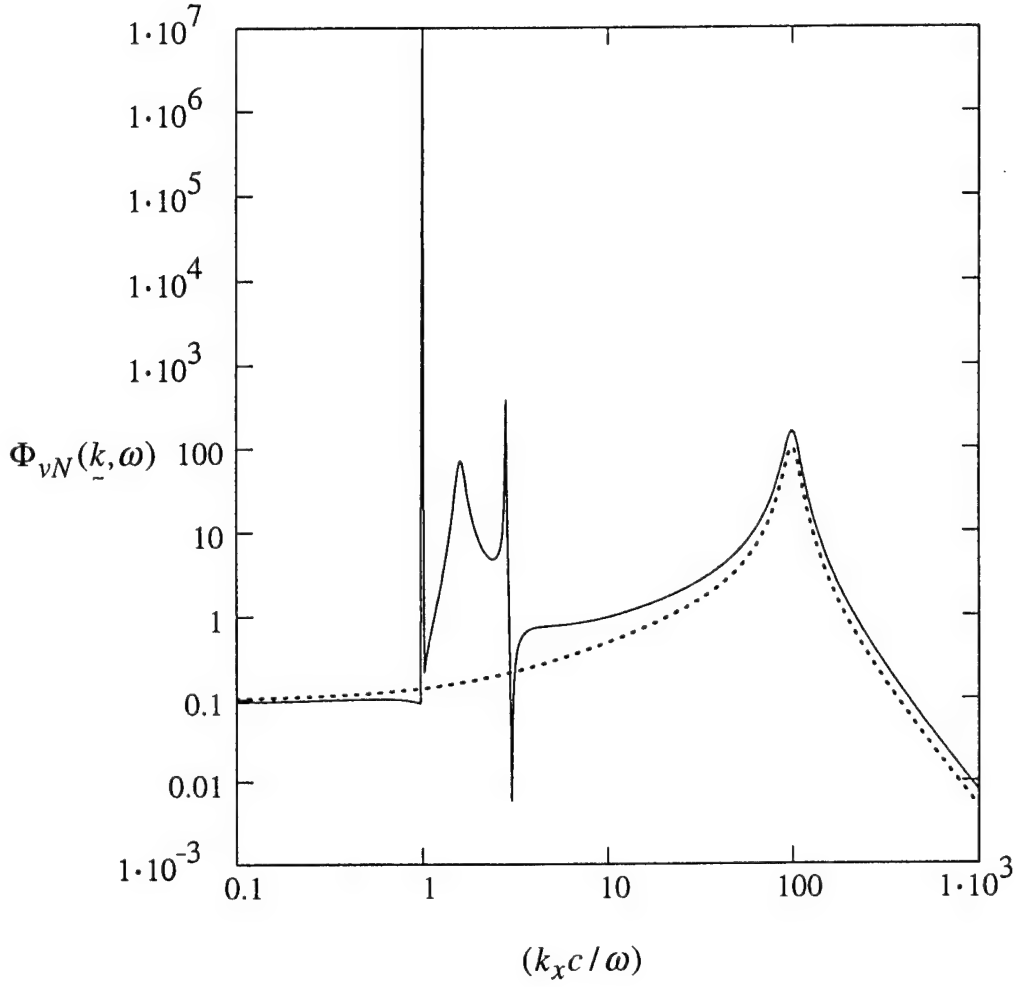

Fig. 13g. The equivalent spectral density $\Phi_{vN}(\underset{\sim}{k},\omega)$ of the pressure in a turbulent boundary layer (TBL), as a function of $(k_x c/\omega)$ with $(k_y c/\omega) \equiv 0$. The parameters (ε_o) and (ε_c) are both set equal to 10^{-1}.
$(\omega_o/\omega) = (\omega_c/\omega) = 8$.

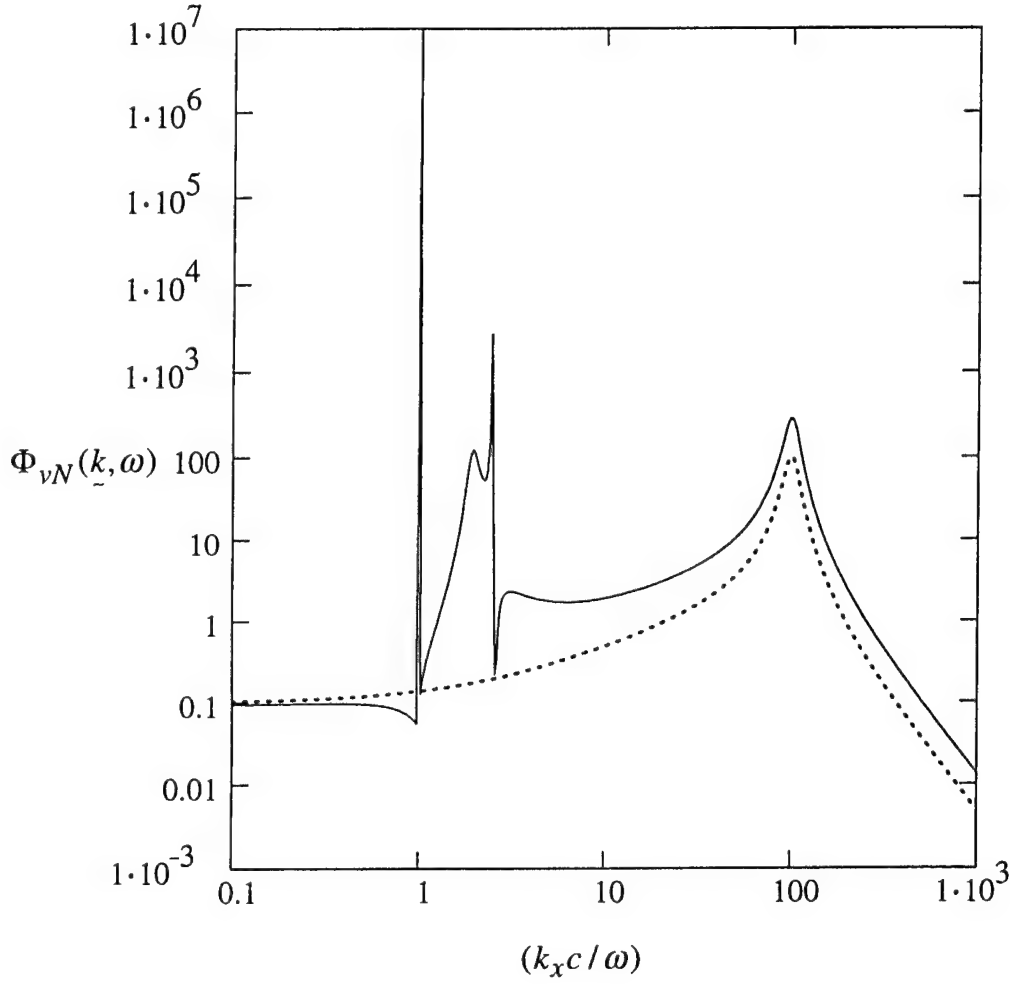

Fig. 13h. The equivalent spectral density $\Phi_{vN}(\underset{\sim}{k},\omega)$ of the pressure in a turbulent boundary layer (TBL), as a function of $(k_x c/\omega)$ with $(k_y c/\omega) \equiv 0$. The parameters (ε_o) and (ε_c) are both set equal to 10^{-1}.
$(\omega_o/\omega) = (\omega_c/\omega) = 6$.

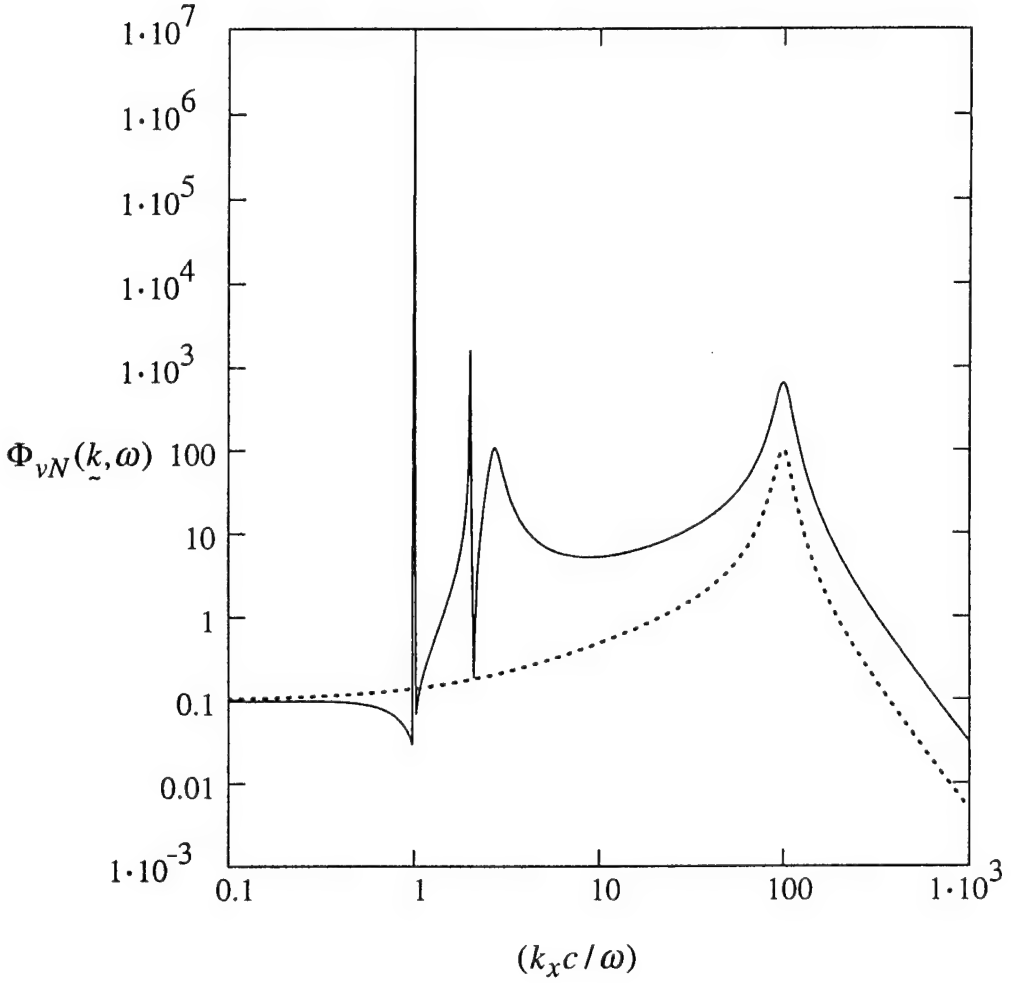

Fig. 13i. The equivalent spectral density $\Phi_{vN}(\underset{\sim}{k},\omega)$ of the pressure in a turbulent boundary layer (TBL), as a function of $(k_x c/\omega)$ with $(k_y c/\omega) \equiv 0$. The parameters (ε_o) and (ε_c) are both set equal to 10^{-1}.
$(\omega_o/\omega) = (\omega_c/\omega) = 4$.

THIS PAGE INTENTIONALLY LEFT BLANK

REFERENCES

1. G. Maidanik and A. J. Tucker, "Acoustic properties of coated panels immersed in fluid media," Journal of Sound and Vibration 34, 519-550 (1974).
2. G. Maidanik, "Proper and first order solution of mechanically constrained panels," Journal of Sound and Vibration 44, 255-256 (1976).
3. G. Maidanik and A. J. Tucker, "Proper and first order solutions of regularly ribbed panels," Journal of Sound and Vibration 44, 267-274 (1976).
4. G. Maidanik, "Surface impedance non-uniformities as wavevector convertors," Journal of the Acoustical Society of America 44, 1062-1073 (1969).
5. G. Maidanik, "Influence of deviations and variations in transducers on the filtering actions of spectral filters," Journal of the Acoustical Society of America 55, 170-189 (1974).
6. G. Maidanik and W. T. Reader, "Filtering action of a blanket dome," Journal of the Acoustical Society of America 44, 497-502 (1968).
7. G. Maidanik and D. W. Jorgensen, "Boundary wave-vector filters for the study of the pressure field in a turbulent boundary layer," Journal of the Acoustical Society of America 42, 494-501 (1967).
8. G. Maidanik, "Flush-mounted pressure transducers as spatial and spectral filters," Journal of the Acoustical Society of America 42, 1017-1024 (1967).
9. G. Maidanik, "Domed sonar system," Journal of the Acoustical Society of America 44, 113-124 (1968).
10. G. Maidanik and T. Eisler, "Reasons and means for measuring the spectral density of the pressure in a subsonic turbulent boundary layer," Journal of Sound and Vibration 84, 39-416 (1982).

11. G. Maidanik, L.J. Maga and Y. F. Hwang, "Modification caused by a compliant coating and a blanket in the velocity and pressure fields induced on a boundary," David W. Taylor Naval Ship Research and Development Center Report SAD-390E-1902 (1982).

12. G. Maidanik, Y. F. Hwang, Y. Liu and L. J. Maga, "Modification in the response caused by introduction of composite layers," David W. Taylor Naval Ship Research and Development Center Report SAD-394E-1902 (1982).

13. Y.F. Hwang, "Mechanics of flow-induced pressure field and modifications by an elastomer layer," NSWC/CD, in-house laboratory independent research digest (1994).

14. G. Maidanik, and J. Dickey, "Resonances of narrow one-dimensional cavities," Journal of Sound and Vibration 136, 105-119 (1990).

INITIAL DISTRIBUTION

Copies	
3	NAVSEA 03T2 2 Taddeo 1 Becker
5	ONR/ONT 1 334 Tucker 1 334 Radlinski 1 334 Vogelsong 1 334 Main 1 Library
4	NRL 1 5130 Bucaro 1 5130 Williams 1 5130 Photiadis 1 Library
4	NUWC/NPT 1 Sandman 1 Harari 1 3332 Lee 1 Library
2	DTIC
2	Johns Hopkins University 1 Green 1 Dickey
1	Applied Physics Lab Johns Hopkins University Library
2	ARL/Penn State University 1 Burroughs 1 Biancardi
1	Cambridge Collaborative Manning
1	Cambridge Acoustical Associate Garrelick
1	J. G. Engineering Research Greenspan
2	MIT 1 Dyer 1 Manning
1	Catholic Uni. of Am. Eng. Dept. McCoy

Copies	
2	Boston University 1 Pierce 1 Barbone
2	Penn State University Koopman
2	Virginia Tech 1 Knight 1 Fuller

Copies	Code	Name
1	01B	Sevik
1	011	Corrado
2	0112	Douglas Halsall
1	20	
1	2040	Everstine
1	2042	Hambric
1	70	Covich
3	7015	Fisher Hamly Vendittis
1	7020	Strasberg
3	7030	
1	7200	Hwang
4	7250	Shang Maga Vasudevan Carroll
1	726	Szilagyi
1	842	Graesser
2	3421	(TIC-Carderock)